THE FERMI RADII OF LITHIUM BY POSITRON ANNIHILATION

by

JOHN JOSEPH PACIGA
B.Sc., University of Guelph, 1969

A THESIS SUBMITTED IN PARTIAL FULFILMENT OF
THE REQUIREMENTS FOR THE DEGREE OF
MASTER OF SCIENCE

in the Department
of
Physics

We accept this thesis as conforming to the
required standard

THE UNIVERSITY OF BRITISH COLUMBIA
April, 1971

In presenting this thesis in partial fulfilment of the requirements for an advanced degree at the University of British Columbia, I agree that the Library shall make it freely available for reference and study. I further agree that permission for extensive copying of this thesis for scholarly purposes may be granted by the Head of my Department or by his representative. It is understood that copying or publication of this thesis for financial gain shall not be allowed without my written permission.

Department of Physics
The University of British Columbia
Vancouver 8, Canada

April 15, 1971

ACKNOWLEDGEMENTS

The author is indebted to Dr. D. Ll. Williams for suggesting the topic of this study and providing supervision throughout its duration.

A number of illuminating discussions and suggestions provided by Jim McLarnon and the late Peter Petijevich is gratefully acknowledged. The former is also to be thanked for technical assistance with the electronics.

A National Research Council Scholarship provided financial assistance for the author during the early stages of this work.

Abstract

A positron annihilation experiment involving collinear point geometry is used to make a direct comparison of the k_{110} and k_{100} Fermi radii in a single crystal of lithium. It is found that k_{110} is greater than k_{100} by 5.6 ± 1.2%, in agreement with theory and a phenomenological interpretation of an earlier long slit experiment. The higher momentum components of the positron wavefunction are calculated by a direct method and found to be negligible. On the other hand, a less straightforward estimate based on a flattened Seitz potential shows that the higher momentum components of the electron wavefunction significantly reduce the experimentally observed anisotropy. Hence, the difference of 5.6% should be regarded as an upper limit on the true distortion of the Fermi surface of lithium.

TABLE OF CONTENTS

LIST OF TABLES

LIST OF FIGURES

CHAPTER I

INTRODUCTION

After DeBenedetti and his colleagues[1] published the first measurements of sufficient angular resolution on gold in 1950, the application of positron annihilation techniques to study the Fermi surface of metals expanded significantly. This flourish of activity was partly a result of the limitations of the more traditional tools of Fermiology. Techniques such as the anomalous skin effect, cyclotron resonance, magnetoresistance, or the de Haas-van Alphen effect require a long mean free path of the electron in the metal, and consequently it is desirable to work at liquid helium temperatures. However, there are two cases in which low temperature experiments are ineffective. The first case is that of disordered alloys for which the mean free path of the electron is short even at low temperatures. Secondly, a number of metallic crystals undergo structure transformations at low temperatures. In both of these instances, positron annihilation studies have a definite advantage as the mean free path does not enter into the analysis.

Lithium is in the second category mentioned above since it undergoes a Martensitic transformation at 78°K from the body-centred cubic structure to the hexagonal close-packed structure. This occurrence is rather unfortunate because

lithium has the simplest electronic structure of any metal and calculations of its band structure are abundant. However, no reliable experimental evidence of its Fermi surface structure existed until the positron annihilation experiments conducted by Donaghy and Stewart in 1964.[2,3,4]

The present study of the Fermi surface of lithium was undertaken for several reasons. The results of Donaghy and Stewart agreed well with a predicted asphericity of about 5% in the Fermi surface of lithium, but it was necessary to rely on a phenomenological model to interpret their results. The present work uses a different experimental geometry which allows a more direct comparison of the radii of the Fermi surface in various crystallographic directions. In addition, it was felt that an independent measurement was desirable both because the asphericity is not appreciably greater than the typical experimental accuracy of positron annihilation experiments (approximately 1%), and also because the results of Donaghy and Stewart were not in agreement with those of certain x-ray experiments.

In this thesis it will be assumed that the reader is familiar with the properties and notation of reciprocal space as discussed in most solid state textbooks. (The first chapter of Ziman's book[5] is adequate for this purpose.) Also, the literature on positron annihilation in metals is so extensive that no attempt will be made to review it exhaustively. For

example, work on other metals will largely be ignored and no details of the physics of the annihilation process will be given. Numerous review articles and lists of references on these topics exist elsewhere.[6,7,8,9]

The material necessary for an understanding of the theory and experiments relevant to this study is contained in Chapter II. Chapter III describes the method used to grow lithium single crystals and it also gives the details of the apparatus used in the actual positron annihilation experiment. The data is presented in Chapter IV and discussed in relation to the existing theoretical and experimental work. Particular emphasis is given to an examination of the higher momentum components of the electron and positron wavefunctions. Finally, Chapter V provides a summary of the conclusions which can be drawn from this study.

CHAPTER II

SUMMARY OF THEORY AND EXPERIMENT

A Basic Principle of Angular Correlation Experiments using Positron Annihilation:

When a positron and an electron annihilate in a metal, two 0.511 MeV gamma rays are emitted at exactly 180° to each other in the centre of mass frame of reference. In the laboratory frame, however, the gamma rays deviate from anticollinearity because of the momentum of the annihilating particles. In an oversimplified interpretation, it is the momentum of the electron before annihilation which causes the deviation from 180° if the positron is assumed to be at rest.

The apparent simplicity of measuring the angular correlation of annihilation radiation to obtain information about the momentum distribution of electrons in metals is immediately evident from the equation relating the transverse momentum of an electron, P_t, and the angle θ by which the two annihilation photons, γ_1 and γ_2, deviate from 180°. Applying the law of conservation of momentum to figure 1 gives

$$P_t = 2mc \cos\alpha$$

where the angle α is defined in the diagram and mc is the momentum associated with each annihilation photon (the rest mass of an electron multiplied by the velocity of light). From the diagram, $\cos\alpha = \cos(90° - \theta/2) = \sin(\theta/2)$, hence

$\alpha = \theta/2 + \beta$

$\beta + \theta = 90°$

$\rightarrow \alpha = 90° - \theta/2$

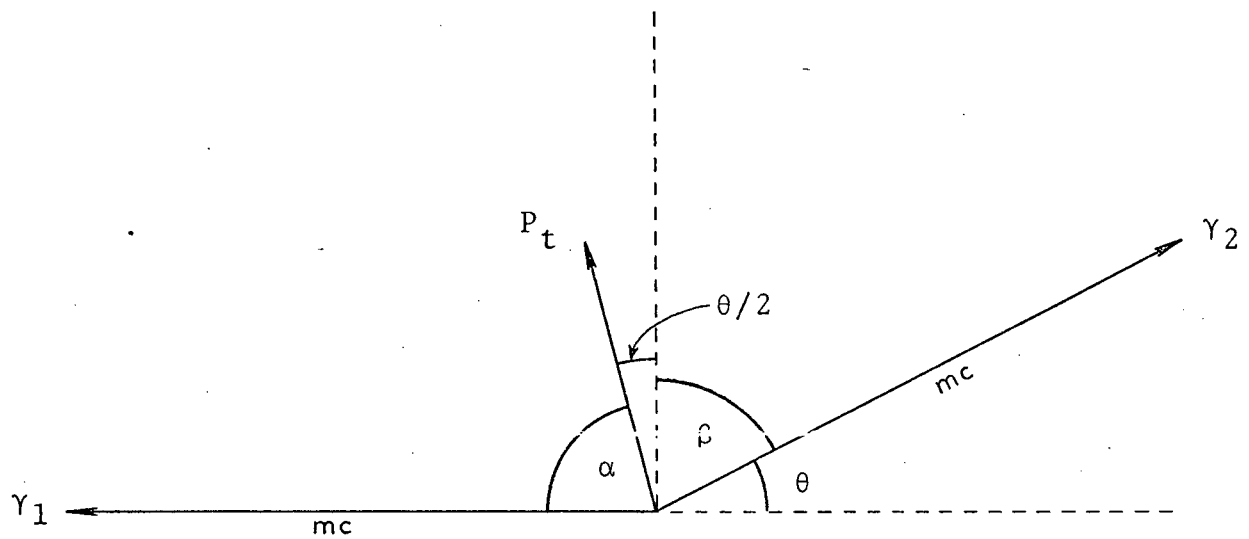

Figure 1: Angular relation between two annihilation photons.

$$P_t = 2mc \sin(\theta/2)$$

Since the deviation from anticollinearity is small (θ is typically less than 20 milliradians), this gives

$$P_t \simeq mc\theta \qquad (1)$$

From this equation, measuring θ should give direct information about the momentum of an electron before annihilation, but in order to extract such information from an experiment several simplifying assumptions are usually made. Perhaps the most significant of these has already been mentioned; namely, that the positron is thermalized or has an energy of approximately 0.025 eV. Consequently, it can be assigned zero momentum so that only the electron is responsible for the deviation of the photons from 180°. Early calculations[10] showed that a positron thermalized in 3×10^{-12} second, a time much shorter than the measured annihilation times[11] which are typically of the order of 2×10^{-10} second. Hence, for any experiment performed at room temperature it is quite safe to assume that the positron is completely thermalized before annihilation.

At low temperatures, however, both theory[12] and experiment[13] indicate that the situation is quite different, and in some cases the positron may annihilate before complete thermalization. A significant result of these studies has been the discovery that positrons attain a minimum possible energy at low temperature. For example, a positron in lithium reaches a

minimum observed energy of approximately 0.017 eV at 200°K and its energy cannot be lowered by a further reduction in temperature. This suggests that the resolution of any positron annihilation experiment has an ultimate limit, since the motion of the positron will blur fine structural details of the Fermi surface.

In using equation (1) to obtain information about the Fermi surface, it is implied that positrons do annihilate with electrons near the Fermi level. Annihilation with core electrons does, in fact, contribute to a broad experimental background, but because the positron is repelled from the positive ion core, this contribution is small for metals like lithium in which the volume of the ion core is small.

Another assumption which simplified the interpretation of early experiments is that the probability of annihilation is independent of the velocity of the electron. That this is not strictly true was made evident by Kahana,[14] who proposed that the annihilation rate for positrons has a momentum dependent enhancement factor, $\varepsilon(\gamma)$, of form

$$\varepsilon(\gamma) = a + b\gamma^2 + c\gamma^4$$

where $\gamma = k/k_F$ and a,b,c are positive constants which depend on the electron density. The enhancement factor is a measure of the increased density of electrons of momentum $\underline{k}$ at the positron and it is evident that the annihilation cross-section increases slightly with increasing electron momentum. In relation to

this it must be assumed that the total momentum of the annihilating pair is not affected by particles around the pair. This is reasonable because the electron-positron pair is electrically neutral and appears to move quite freely through the lattice.[15]

B Momentum Distributions in Angular Correlation Experiments:

The observed momentum distribution resulting from the annihilation pairs can be expressed in mathematical terms as follows. In an independent particle approximation which neglects many-body effects, the probability $\rho_{\underline{k}}(\underline{K})$ that an electron with wavevector $\underline{k}$ will annihilate with a thermalized positron and yield a photon pair with momentum $\underline{p} = \hbar\underline{K}$ is proportional to[1,16]

$$\left| \int_{\text{crystal}} \psi(\underline{k},\underline{r})\ \phi_+(\underline{r})\ e^{-i\underline{K}\cdot\underline{r}}\ d\underline{r} \right|^2$$

where $\psi(\underline{k},\underline{r})$ and $\phi_+(\underline{r})$ are the electron and positron wavefunctions at position $\underline{r}$. The observed momentum distribution $\rho(\underline{K})$ of the photon pairs is proportional to a sum over all occupied states in $\underline{k}$-space, including core states:

$$\rho(\underline{K}) = C \sum_{k \leq k_F} \left| \int_{\text{crystal}} \psi(\underline{k},\underline{r})\ \phi_+(\underline{r})\ e^{-i\underline{K}\cdot\underline{r}}\ d\underline{r} \right|^2 \qquad (2)$$

where $C = \alpha^3/4\pi^2$, $\alpha = 1/137$, and k_F is the Fermi radius. The above equation is valid for angular momentum $\ell=0$, but Mijnarends[17] has determined it for the more general anisotropic case of $\ell\neq 0$. To obtain the actual number of photon pairs

emitted into a region of $\underline{k}$-space, one attempts to integrate the annihilation probability $\rho(\underline{K})$ over the region of interest.

It is immediately evident that a precise analysis of the angular correlation curves requires a detailed knowledge of the two wavefunctions $\psi(\underline{k},\underline{r})$ and $\phi_+(\underline{r})$. To a first approximation the positron wavefunction can be considered constant. This assumption is reasonable everywhere except in the ion core region where $\phi_+(\underline{r})$ is essentially zero, and therefore it is particularly good in metals such as lithium in which the core occupies only 6% of the volume of the unit cell. A detailed analysis of the effect of both the positron and electron wavefunctions on the angular distributions in silicon and aluminum has been performed by Stroud and Ehrenreich[18] with excellent results. These authors have determined single particle wavefunctions for positrons in solids by utilizing the close relationship of x-ray form factors to the Fourier coefficients of the potential seen by the positron. A more complete discussion of their method will be given in Chapter IV.

For the electron wavefunction, the simplest case which can be considered is that of the free electron theory of Sommerfeld in which the atom lattice is completely ignored and the electrons are considered to be a gas of non-interacting particles restricted only by the boundaries of the metal and the Pauli exclusion principle. The electron wavefunction is simply a plane wave

$$\psi(\underline{k}) = 1/\sqrt{V}\ e^{i\underline{k}\cdot\underline{r}}$$

where V is the volume of the metal. The energy of an electron state is represented by the free electron parabola

$$E(\underline{k}) = \frac{\hbar^2 k^2}{2m} .$$

At 0°K all states are completely filled up to the Fermi level, beyond which the occupation number drops abruptly to zero. The constant energy surface at which this occurs defines the Fermi sphere of radius k_F

$$E_F = \frac{\hbar^2 k_F^2}{2m} .$$

The free electron theory predicts angular correlation curves remarkably well, even though it fails completely in predicting positron lifetimes in metals.[19] The reason is mainly that it ignores the electron-positron attraction which enhances the electron density at the positron and reduces its lifetime. This theory will, however, be sufficient to explain the experimental geometries used in positron annihilation experiments, and a discussion of the more refined approximations to the electron wavefunction will be deferred to a later section. It is sufficient to note at this point that if the free electron wavefunction is substituted into equation (2) with $\phi_+(\underline{r})$ = constant, then $\rho(\underline{K}) = \rho(K)$ is spherically symmetric, equal to a constant inside the Fermi sphere, and equal to zero outside.

C Experimental Geometries:

(i) Long slit geometry

The experimental arrangement used by all early investigators to study the angular correlation of annihilation radiation is termed the long slit geometry. The sample is placed midway between two gamma ray detectors which are positioned behind a set of horizontal lead slits as shown in figure 2(a). An external source such as sodium-22 can be used to shine positrons onto the sample, or the sample itself can be a source of positrons as in the case of neutron irradiated copper-64.

The slits on one side of the apparatus can be raised to define an angle at the sample of $\theta = z/D$ where z is the distance raised and D is one half the distance between the detectors. It is evident that the geometrical resolution of such an arrangement is related to the width of the slits and the distance D to the sample.

The number of photons with a well defined z-component measured with the long slit geometry is given by

$$N(K_z) \propto \int_{-\infty}^{\infty} \int_{-\infty}^{\infty} \rho(\underline{K})\, dK_x dK_y \qquad (3)$$

where $K_z = mc\theta/\hbar$ from equation (1). The integral in the x-direction is a result of the fact that the slits are wider in this direction than the angle corresponding to the width of the Fermi surface, and the integral over the y-direction arises because the Doppler shift in energy due to the momentum of the

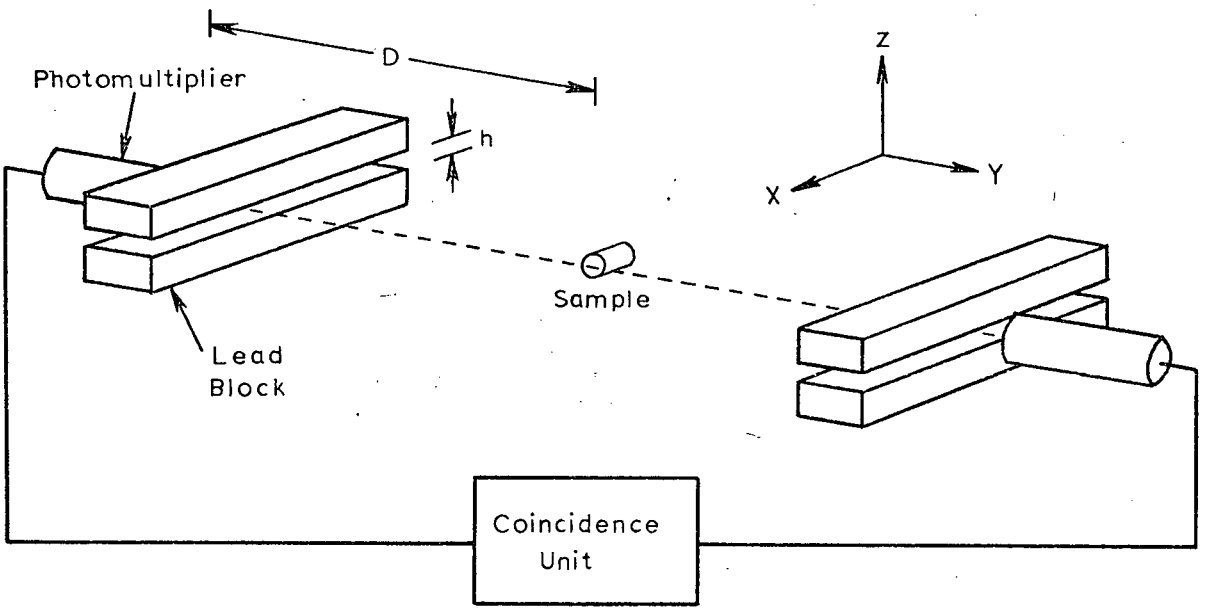

Figure 2(a): Long slit apparatus.

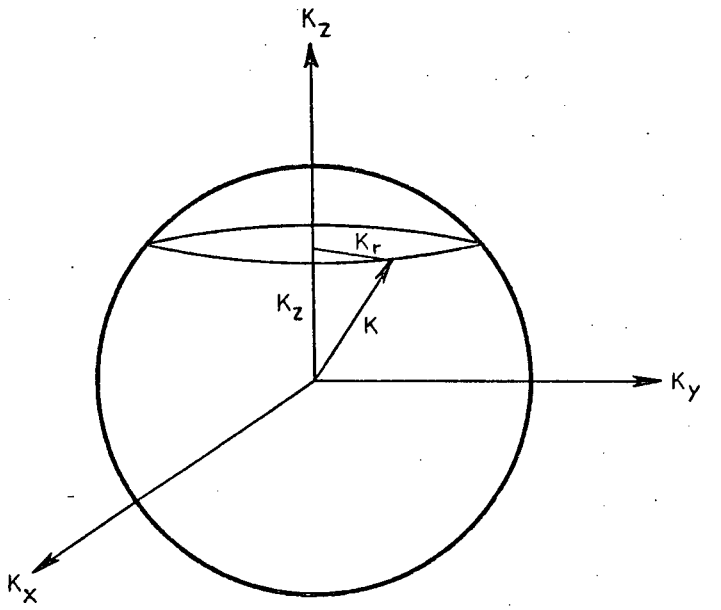

Figure 2(b): Region of Fermi sphere sampled by long slit apparatus.

annihilating pair cannot be detected.

As stated previously, the momentum distribution of equation (2) is generally anisotropic because of many-body effects and the presence of the lattice potential; however, for simplicity the present discussion will be restricted to the free electron case. Hence equation (3) becomes

$$N(K_z) \propto \rho(K) \int_{-\infty}^{\infty} \int_{-\infty}^{\infty} dK_x dK_y$$

which is proportional to the area of a slice of the Fermi sphere at constant K_z as shown in figure 2(b). Using the fact that

$$K^2 = K_x^2 + K_y^2 + K_z^2 = K_r^2 + K_z^2 ,$$

the integral can be transformed to

$$N(K_z) \propto 2\pi \rho(K) \int_{0}^{\infty} K_r dK_r .$$

Since $KdK = K_r dK_r$ for K_z = constant, this becomes

$$N(K_z) \propto 2\pi \rho(K) \int_{K_z}^{\infty} KdK$$

But $\rho(K) = 0$ if K_z is greater than the Fermi radius k_F, thus

$$\begin{aligned} N(K_z) &\propto k_F^2 - K_z^2 && \text{for } K_z \leq k_F \\ N(K_z) &= 0 && \text{for } K_z > k_F \end{aligned} \qquad (4)$$

Equation (4) is the inverted parabola which characterizes angular correlation experiments using the long slit geometry.

The sharp cut-off in the curve at the Fermi radius is unshifted even with the inclusion of many-body effects such as the electron-positron interaction.[19] In an actual experiment the free electron parabola is superimposed on a much broader background which arises from such effects as chance coincidences, core annihilations, and higher momentum components of the electron and positron wavefunctions. These higher momentum components, along with the actual shape of the Fermi surface, significantly affect the form of the angular correlation curves.

(ii) Point geometry and the Rotating Specimen Method

In the point geometry arrangement which was introduced in the 1960's,[20,21,22] the width of the slit is reduced in the x-direction in order to define two components of momentum instead of just one. This arrangement is illustrated in figure 3(a); the region of $\underline{k}$-space sampled by the detectors being the chord of figure 3(b).

Assuming the free electron case as before, equation (3) becomes

$$N(K_z) \propto \rho(K) \int_{-\infty}^{\infty} dK_y$$

or, $$N(K_z) \propto \rho(K) \int_{0}^{\infty} dK_r$$

where K_r is the semi-chord shown in figure 3(b). Proceeding as in the long slit case, $KdK = K_r dK_r$ for constant K_z, and changing

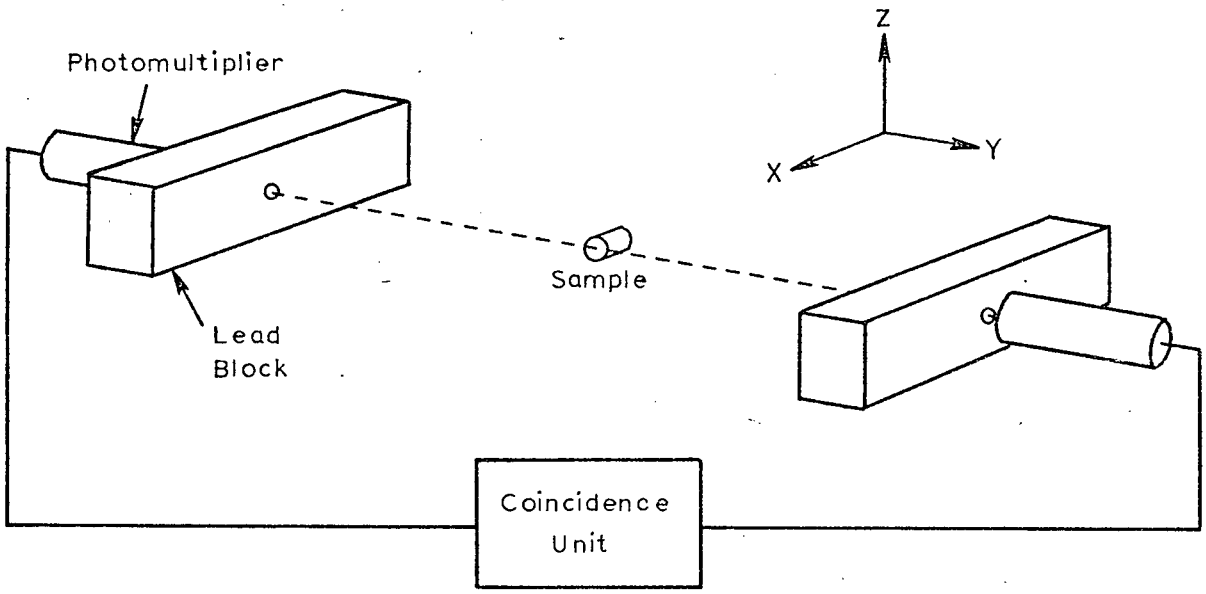

Figure 3(a): Point geometry apparatus.

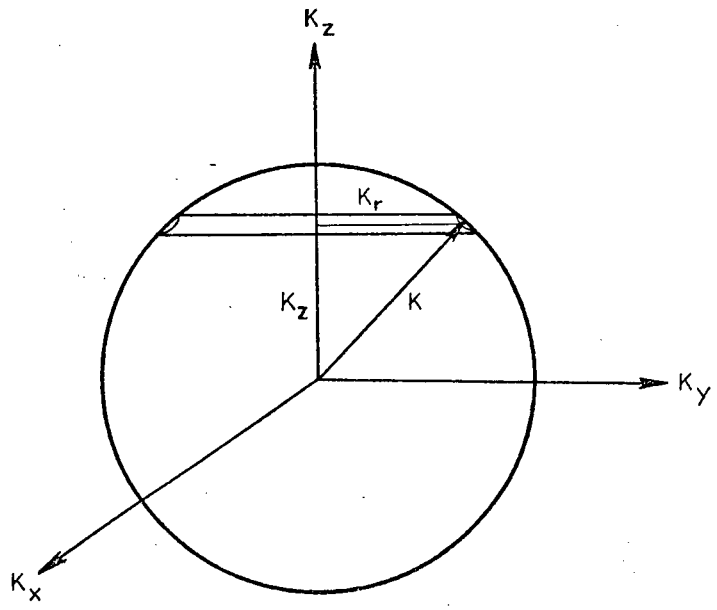

Figure 3(b): Region of Fermi sphere sampled by point geometry apparatus.

to the appropriate limits the integral becomes

$$N(K_z) \propto \rho(K) \int_{K_z}^{\infty} \frac{KdK}{K_r}$$

or, $$N(K_z) \propto \rho(K) \int_{K_z}^{\infty} \frac{d(K^2 - K_z^2)}{\sqrt{K^2 - K_z^2}} .$$

Integrating from K_z to the Fermi level k_F, the result is

$$N(K_z) \propto \sqrt{k_F^2 - K_z^2} . \qquad (5)$$

Since $K_z = mc\theta/\hbar$ from equation (1), the angular correlation curve for the point geometry arrangement is elliptical (or circular for a suitable choice of axes). The advantage of this geometry is that another component of momentum is defined; however, there is a corresponding drop in the coincidence count rate because of the narrower slits.

If $\theta=0$ it is obvious from equation (5) that the number of counts is directly proportional to the radius of the Fermi sphere, k_F. If the Fermi surface is actually anisotropic, rotation of the crystal with the detectors at $\theta=0$ will map out a comparison of the 'diameters' of the Fermi surface for different directions. This method is termed the collinear point geometry or rotating specimen method and was used independently by Williams, et al.[22] and Sueoka[23] to study the Fermi surface of copper.

In the collinear point geometry the crystal must be made

cylindrical to avoid anisotropies arising from gamma ray absorption. It should also be noted that the curves obtained by rotating the crystal cannot give a value for the amount of annihilation with core electrons. This information must be obtained from theoretical calculations or from a regular sideways experiment ($\theta \neq 0$) using either the long slit or point geometry.

D Band Structure Calculations & the Fermi Surface of Lithium:

(i) Nearly Free Electrons

In real metals, the presence of the lattice potential necessitates the use of a more sophisticated approximation to the electron wavefunction than is given by the free electron model. Many such approximations have been developed, but only a brief introduction to two of the simpler ones, the nearly free electron (NFE) theory and the orthoganalized plane wave (OPW) method will be given here. Several good references [5, 24,25,26] are available for further details on these and other more refined techniques such as pseudopotential theory, cellular methods, augmented plane waves (APW's), and the Green's function method.

A great deal of understanding about the behaviour of electrons in metals can be obtained by applying first order perturbation theory to free electrons. In the NFE approximation the inner or core electrons are considered to be tightly

bound to the nucleus, and the conduction electrons behave as nearly free but subject to Bragg reflections at the Brillouin zone boundaries because of the presence of a weak periodic potential $V(\underline{r})$.

No exact solution exists for the related Schrödinger equation

$$\left(-\frac{\hbar^2}{2m}\nabla^2 + V(\underline{r})\right)\psi(\underline{r}) = E(\underline{k})\,\psi(\underline{r})$$

but to first order perturbation theory the energy of an electron state can be represented by (Ref. 5, page 70):

$$E(\underline{k}) = \frac{\hbar^2 k^2}{2m} + \langle \underline{k}|V(\underline{r})|\underline{k}\rangle + \sum_{\substack{k \\ k\neq k'}} \frac{|\langle \underline{k}|V(\underline{r})|\underline{k}'\rangle|^2}{\frac{\hbar^2}{2m}\{\underline{k}^2 - \underline{k}'^2\}} .$$

The matrix element for scattering from state $\psi_{\underline{k}}$ to $\psi_{\underline{k}'}$ is

$$M_{\underline{k}'\underline{k}} = \langle \underline{k}|V(\underline{r})|\underline{k}'\rangle$$

$$= \int \psi^*_{\underline{k}'}(\underline{r})\, V(\underline{r})\, \psi_{\underline{k}}(\underline{r})\, d\underline{r}$$

where the periodic potential $V(\underline{r})$ can be expanded in a Fourier series in reciprocal lattice vectors $\underline{G}$:

$$V(\underline{r}) = \sum_{\underline{G}} V_{\underline{G}}\, e^{i\underline{G}\cdot\underline{r}}$$

with coefficients

$$V_{\underline{G}} = \frac{1}{V}\int V(\underline{r})\, e^{-i\underline{G}\cdot\underline{r}}\, d\underline{r} . \qquad (6)$$

As usual, V is the volume of the metal. It can be shown (Ref. 5, page 51) that the matrix elements are equal to $V_{\underline{G}}$ if $\underline{k} - \underline{k}'$

equals a reciprocal lattice vector and are zero otherwise. Hence,

$$E(\underline{k}) = \frac{\hbar^2 k^2}{2m} + V_o + \sum_{\substack{G \\ G \neq 0}} \frac{|V_{\underline{G}}|^2}{\frac{\hbar^2}{2m}\{\underline{k}^2 - (\underline{k}-\underline{G})^2\}}$$

where $V_o = \langle \underline{k} | V(\underline{r}) | \underline{k} \rangle$.

The potential V_o is a correction for the mean potential energy of an electron in the lattice. This result does not differ greatly from the free electron case if the Fourier coefficients of the potential, $V_{\underline{G}}$, are small and if $\underline{k}$ does not approach $\underline{k}-\underline{G}$ in value (that is, if $\underline{k}$ does not approach a Brillouin zone boundary). Consequently, the wavefunction of an electron in the conduction band will differ only slightly from a single plane wave except at points near the zone boundary.

The above condition for nonvanishing matrix elements is identical to the condition for Bragg reflection. The introduction of a Bragg plane outside the free electron sphere mixes a reflected component into an otherwise single plane wave, thereby linking states which differ by a reciprocal lattice vector $\underline{G}$. In order to find a solution near a zone boundary, one assumes that the wavefunction may be expanded in a series of form

$$\psi(\underline{k},\underline{r}) = \sum_{\underline{G}} a_{\underline{G}}(\underline{k})\ e^{i(\underline{k}-\underline{G})\cdot\underline{r}} \qquad (7)$$

which can be substituted into the Schrödinger equation. Such

a wavefunction is said to contain higher momentum components because it involves terms with momenta greater than $\underline{k}$. This expansion does not imply that the true wavefunctions ressemble plane waves, but the energies obtained by using such an expansion are physically realistic. Ignoring all coefficients except $a_o(\underline{k})$ and $a_{-\underline{G}}(\underline{k})$, this becomes

$$\psi(\underline{k},\underline{r}) = a_o(\underline{k})\ e^{i\underline{k}\cdot\underline{r}} + a_{-\underline{G}}(\underline{k})\ e^{i(\underline{k}-\underline{G})\cdot\underline{r}}\ .$$

One then solves the secular equation

$$\begin{vmatrix} \frac{\hbar^2k^2}{2m} - E(\underline{k}) & V_{\underline{G}} \\ V^*_{\underline{G}} & \frac{\hbar^2}{2m}(\underline{k}-\underline{G})^2 - E(\underline{k}) \end{vmatrix} = 0$$

to obtain the following quadratic expression for the energy:

$$E(\underline{k}) = \frac{1}{2}\left(\frac{\hbar^2k^2}{2m} + \frac{\hbar^2}{2m}(\underline{k}-\underline{G})^2\right) \pm \frac{1}{2}\left(\left|\frac{\hbar^2k^2}{2m} - \frac{\hbar^2}{2m}(\underline{k}-\underline{G})^2\right|^2 + 4|V_{\underline{G}}|^2\right)^{1/2} \quad (8)$$

It is evident that the two degenerate, unperturbed states which were separated by a reciprocal lattice vector are now split in energy. The perturbation has the greatest effect near the Brillouin zone boundary $\underline{k} = \pm 1/2\underline{G}$ at which point

$$E(\underline{k}) = \frac{\hbar^2k^2}{2m} \pm |V_{\underline{G}}|$$

Away from the zone boundary the energy is not too different from the free electron parabola if the perturbing potential is small.

The constant energy surfaces are thus distorted from their unperturbed form only near the Brillouin zone faces where the distortion at $\underline{k}$ arises via a single Fourier coefficient of the lattice potential between a free electron state at $\underline{k}$ and another such state at $\underline{k}-\underline{G}$. The familiar result of equation (8) is depicted in the extended zone scheme in figure 4. In one dimension, the free electron parabola exhibits gaps at the Brillouin zone boundaries of magnitude $2|V_{\underline{G}}|$.

Since the true crystal potential is not weak, the success of the nearly free electron model is at first sight rather surprising. Insight to its success has been provided by pseudopotential theory. Essentially, the effective pseudopotential seen by the valence electrons is weak because the requirement that the wavefunctions of valence electrons be orthogonal to core states has the effect of introducing a repulsive pseudopotential which partially cancels the true crystal potential.

(ii) Orthogonalized Plane Waves

In practice, the nearly free electron method can be applied to very few metals because an expansion in plane waves requires a large number of terms to duplicate the sharp oscillations of the atomic wavefunctions in the neighbourhood of the ions. Much more rapid convergence is obtainable with the OPW method developed by Herring.[27]

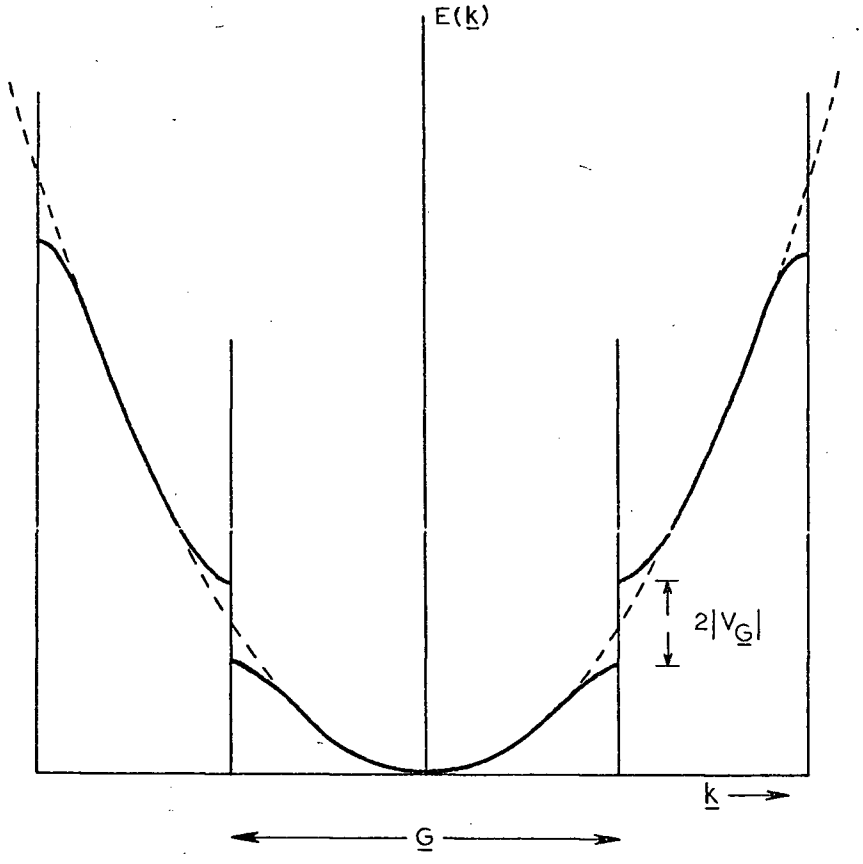

Figure 4: Splitting of energy levels in extended zone scheme (one dimension).

In this method the wavefunction of the valence electrons is assumed to have an expansion of the form

$$\psi_{\underline{k}} = \sum_{\underline{G}} a_{\underline{k}+\underline{G}} \chi_{\underline{k}+\underline{G}}$$

where the basis states $\chi_{\underline{k}}$ are plane waves from which are subtracted a linear combination of core states $\phi_{j\underline{k}}$:

$$\chi_{\underline{k}} = \frac{1}{\sqrt{V}} e^{i\underline{k}\cdot\underline{r}} - \sum_{j} b_j \phi_{j\underline{k}}$$

The coefficients b_j are

$$b_j = \langle \phi_{j\underline{k}} | 1/\sqrt{V}\ e^{i\underline{k}\cdot\underline{r}} \rangle$$

so that the conduction electron wavefunction is orthogonal to the core states, i.e.,

$$\langle \phi_{j\underline{k}} | \psi_{\underline{k}} \rangle = 0 \ .$$

This orthogonality condition may be considered a direct result of the Pauli exclusion principle. The core states themselves are highly localized atomic orbitals which may be represented in the tight binding approximation as

$$\phi_{j\underline{k}}(\underline{r}) = \frac{1}{\sqrt{N}} \sum_{\underline{R}} e^{i\underline{k}\cdot\underline{R}} \phi_j(\underline{r}-\underline{R}) \ .$$

ϕ_j is the core state with quantum numbers j = (n,l,m), and the sum extends over N lattice sites each separated by a direct lattice vector $\underline{R}$.

The orthogonalized plane waves $\chi_{\underline{k}}$ resemble plane waves in the regions between ions and are orthogonal to all core states. This strong modulation at the nuclei makes convergence of an

OPW expansion quite rapid, and a single OPW can give a useful first approximation to the band structure of about 25 simple metals and semi-metals. Only two or three OPW's are needed to estimate the band structure in the very corners of the Brillouin zone. It should be noted, however, that the wavefunctions are not precise eigenfunctions of the given Hamiltonian, therefore one cannot obtain solutions of arbitrary accuracy by increasing the number of terms in the expansion.[28]

(iii). Band Calculations in Lithium

Since lithium has the simplest electronic structure of any metal (two highly localized 1-s core electrons and one nearly free 2-s conduction electron), it has been used as a test case for nearly every type of band calculation. In fact, lithium[29] and sodium[30] were the metals chosen for the first realistic band calculations performed by Wigner and Seitz in the early 1930's.

Since lithium crystallizes in the body-centred cubic structure, its first Brillouin zone is the regular rhombic dodecahedron illustrated in figure 5. The free electron sphere occupies only one half the volume of the first Brillouin zone since lithium has one conduction electron associated with each atom, and because of the Pauli principle two are required to fill all the states in the first zone. From the nearly free electron model one would expect that the free electron sphere

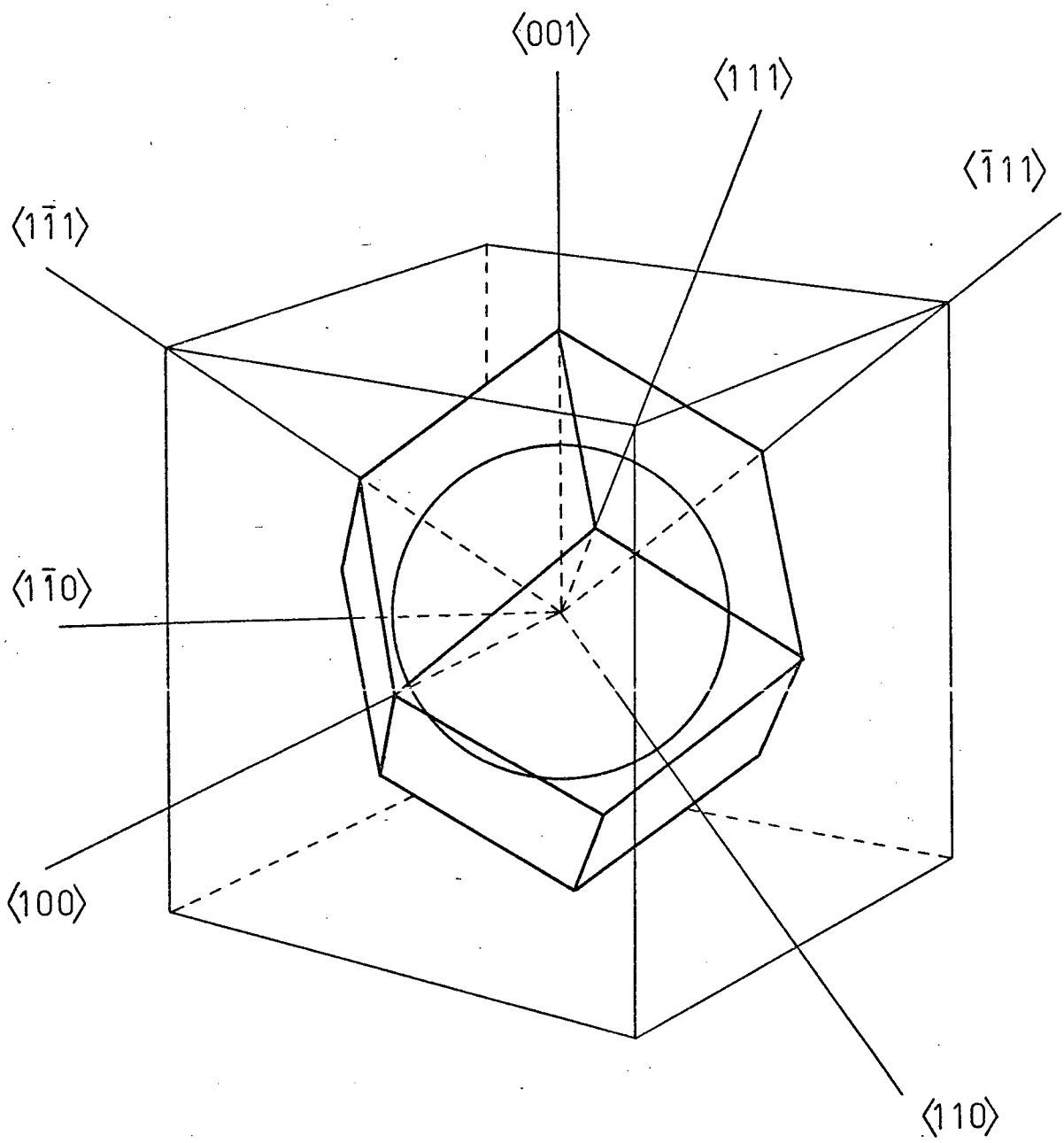

Figure 5: First Brillouin Zone of Lithium showing Free Electron Sphere.

would be distorted by the presence of the Bragg reflection planes (Brillouin zone surfaces). Distortion will be greatest in directions for which the sphere is closest to the zone faces; in this case in the twelve <110> directions.

In order to obtain an idea of the shape of the Fermi surface of lithium, Glasser and Callaway[31,32,33] have calculated the band structure using the OPW method in conjunction with an empirical potential constructed by Seitz. It was found that the Fermi surface is close to being spherical but has small bulges in the <110> directions of the order of 5% of the radius. Their value for the Fermi energy is listed in table 1 along with the results obtained by other investigators who used different methods.

By far the most extensive calculations of the energy bands in alkali metals were carried out by Ham[34,35] using the quantum defect method. This procedure does not require the explicit construction of a potential and automatically takes into account exchange, correlation, and relativistic effects in the interaction of valence electrons with core electrons. Ham also found that the Fermi radius of lithium is increased by some 5% in the <110> direction as compared with the <111> and <100> directions. This distortion is not nearly enough to cause contact with the Brillouin zone face even when the lattice is compressed significantly.

The use of a procedure similar to the augmented plane wave

Table 1

INVESTIGATOR	LATTICE CONSTANT	E_F	COMMENTS
Callaway (32,33)	6.5183 a.u.	-0.427 Ry.	OPW method. Small bulges in the Fermi surface of about 5% in <110> directions. No contact with zone face.
Ham (34,35) quoted in (28)	6.651 6.5183	-0.433 -0.430	Quantum defect method. Gives 5% bulges in <110> directions. No contact.
Schlosser & Marcus (28)	6.5183	-0.429	Method similar to APW. Bulges out by 4.4% in <110> directions & is depressed by 2.7% in <100> directions. No contact.
Capek (37)	6.614	-0.435	Model potential. Elongated in <110> directions. In other directions a few % smaller than free electron sphere. No contact.

Notes:

(a) Atomic units are used with $e=\hbar=1$, $m=1/2$ (see ref. 26, pg. 55). The unit of length is the Bohr radius of hydrogen (0.52917 Å), and the unit of energy is the Rydberg (13.6049 eV).

(b) The Fermi energy in a spherical approximation is -0.422 Ry. The zone boundary in the <110> direction is at -0.412 Ry. and contact occurs if the Fermi energy is greater than this value.

(APW) method leads to results which are in substantial agreement with the previous authors. Using a flattened Seitz potential, the calculations of Schlosser and Marcus[28] indicate a slightly larger outward bulge of about 7% in the <110> directions. This method differs from the cellular method, Green's function method, and the OPW method in that a composite representation of the wavefunction is used instead of an expansion in a single set of wavefunctions obtained by orthogonalising to core state functions. In the original APW method, for example, an expansion in plane waves is used in the outer part of the cell and an expansion in spherical waves is used in the inner part.

Antoncik[36] has employed a pseudopotential method and achieved agreement with Glasser and Callaway by using the same lattice constant and potential. Capek[37] also reports agreement (see table 1). He bases his calculations on a model potential in the form of spherical ℓ-dependent wells. This use of non-local model potentials is similar to, but not quite the same as the pseudopotential method. The technique was used earlier by Heine and Abarenkov[38] who also found that the Fermi surface of lithium behaved as mentioned previously.

It is evident that there is substantial agreement among the different theoretical calculations for lithium. A quite remarkable fact which appears from these calculations is that the band structure does not appear to be very sensitive to

uncertainties in the potential, since significant differences exist in the choices of the various authors.

Despite this agreement, there are several suggestions that the theory developed may not be accurate in all respects. Some early work,[39,40] for example, indicated a considerable amount of contact with the zone faces. Also, Cornwall and Wohlfarth[41] have developed an energy band interpolation scheme based on Glasser and Callaway's results, and they suggest that although the Fermi surface does not appear to touch the zone boundary, the difference is only 0.025 Ry. which is within the accuracy of ±0.05 Ry. stated by Glasser and Callaway. On the other hand, it has been found that the Fermi surfaces of the other alkali metals are considerably less distorted than predicted by Ham's calculations.[38,42]

Several other relevant theoretical papers will be discussed after an examination of the experimental work which has been performed on lithium single crystals.

E Experimental Results of Donaghy and Stewart:

The most definitive experimental determination of the Fermi surface of lithium to date was carried out by Donaghy and Stewart.[2,3,4] A long slit apparatus was used to study the angular distribution of annihilation radiation from crystals oriented in the <110>, <111>, and <100> directions. The resulting experimental curves were significantly different for

the three orientations, and by constructing a phenomenological model with several adjustable parameters, Donaghy and Stewart were able to determine that the Fermi surface of lithium is anisotropic, with the radius k_{110} greater than k_{100} by about 5% as predicted theoretically. It was also determined that the Fermi surface does not contact the zone boundary in the <110> direction unless it does so by an unrealistically narrow neck.

The model which these authors chose was a sphere with twelve bumps superimposed towards the zone faces in the <110> directions. The calculated curves agreed quantitatively with the measured momentum distributions in the region $0<\theta<2.5$ milliradians but differed for $\theta>2.5$ milliradians. The discrepancy for $\theta>2.5$ milliradians was attributed to the fact that some of the photon pairs arise from Umklapp processes and therefore involve higher momentum components of the electron wavefunction. The observed distribution is proportional to the areas of slices through the Fermi surface if $\underline{p} = \hbar\underline{k}$, but not if higher momentum components $\underline{p} = \hbar(\underline{k}+\underline{G})$ are involved.

These particular experimental results have been discussed from a theoretical viewpoint by Melngailis and DeBenedetti.[43] Applying an abbreviated form of the OPW method used by Callaway, they found that the numerically calculated angular correlation curves showed anisotropies in agreement with the statements of Donaghy and Stewart. It was necessary to include both the effect of the shape of the Fermi surface and the effect of the

departure of the electron wavefunction from a single plane wave: the anisotropies could not be explained by the shape alone. In addition, these authors computed the momentum distribution resulting from annihilation with the two core electrons in lithium. For the long slit geometry, a broad, flat curve results which is about one order of magnitude smaller than the conduction electron contribution. Better quantitative agreement with the experimental curves could be obtained by including Kahana's enhancement factor which allows for the electron-positron interaction.

Another possible interpretation of the results of Donaghy and Stewart has been suggested by Stachowiak.[44] If the theory which Mijnarends[17] derived to determine anisotropic momentum distributions in positron annihilation experiments is applied to Donaghy and Stewart's results, the evidence suggests a possibility of contact with the Brillouin zone face in the <110> direction. This is inferred from the fact that the density of states curve derived from Mijnarends theory does not drop to zero at the zone boundary. However, it appears that more experimental orientations are necessary to define this result more accurately, because one must determine an expansion in Kubic harmonics and the results of Donaghy and Stewart only allow the determination of three terms in this expansion.

F Other Methods used to study Lithium:

As stated in Chapter I, the usual low temperature techniques such as the de Haas-van Alphen effect cannot be used to study lithium because it has a phase transition at 78°K. However, several experiments utilizing x-rays can be performed at room temperature and have an advantage over positron annihilation in that no assumptions need be made about positron wavefunctions, thermalization times, or electron-positron interactions.

In particular, Compton scattering has been used to study lithium[45,46,47] since the theoretical Compton profile shows a discontinuity at the Fermi surface similar to the one found in positron annihilation experiments. In a study which also included several other substances, Phillips and Weiss[46] found that their results for polycrystalline lithium yielded values for the Fermi momentum of 0.593 ± 0.015 (a.u.)$^{-1}$ for lithium and 0.509 ± 0.02 (a.u.)$^{-1}$ for sodium, whereas the free electron values are 0.588 and 0.481 respectively. In contrast, positron annihilation experiments yield momentum distributions which are closer to free electron theory. The discrepancy for sodium is especially puzzling since de Haas-van Alphen experiments[48] indicate that the Fermi surface of sodium is spherical to a precision greater than one part in one thousand. Also, the results of Phillips and Weiss for a single crystal of lithium do not agree with Donaghy and Stewart's positron results, since

no deviation from spherical symmetry was found in the <110>, <100>, and <111> directions within their stated accuracy of 3%.

Another method of obtaining information about the Fermi surface is through the soft x-ray emission spectrum. If vacancies are created in the K-shell of lithium by fast electrons, these vacancies are filled by electrons from the conduction band. The energy of the soft x-ray emitted is

$$\hbar\omega = E(\underline{k}) - E_c$$

where the energy of the core states, E_c, is well defined and $E(\underline{k})$ is the energy of an electron in state $\underline{k}$. Unfortunately, this picture is oversimplified, and results for lithium[49] are mainly qualitative since actual experiments are difficult to interpret reliably.[50] It is found that the shape of the spectrum is puzzling in the case of lithium, but is reasonably well understood in sodium and potassium. Ham (ref. 35, page 2539) suggests that the spectrum may indicate that the Fermi surface of lithium contacts the Brillouin zone face, and this discrepancy between positron annihilation experiments and the x-ray results is still unresolved.

It is obvious that both of the methods discussed above are useful only for light metals. In the first case both core and conduction electrons scatter equally, and in the second case the K-shell can be filled from any level above it, therefore interpretation becomes difficult if several higher levels are occupied. Even more important is the fact that good

resolution is difficult to obtain in x-ray experiments. In Compton scattering, for example, there is a characteristic broadening of the Compton profile which has been attributed to the possibility that the experimental curve contains more high momentum than the theoretical curve;[47] however, this broadening may actually be caused by the fact that a weaker band from x-ray Raman scattering overlaps with the Compton profile.[51]

CHAPTER III

SAMPLE PREPARATION AND EXPERIMENTAL APPARATUS

A Sample Preparation:

(i) Crystal growth

Although attempts to grow single crystals of lithium were made as early as 1917 when Hull[52] was determining the structures of various elements by x-ray diffraction, it was not until 1958 that crystals of reasonable size were grown by Nash and Smith.[53] At about the same time, Champier[54] developed a slightly different method using a slow cooling rate of 2 C°/hour to grow single crystals which were 3 millimeters thick and a few square centimeters in area. However, the technique of Nash and Smith with its faster cooling rate of 30 C°/hour has been preferred by subsequent investigators,[55,56,57] and it is a slightly improved version[56] of their method which is used here.

The crystals were grown by a modified Bridgman technique using the three-section crucible shown in figure 6. The bottom section is a growing cup made from a 2-1/4 inch length of 1/2 I.D. seamless stainless steel pipe wrapped with asbestos insulation over which is wound nichrome heater wire in such a way that the hottest portion of the cylinder is at the bottom. Current through the wire is controlled manually by means of a variac. The middle section is a mild steel plunger which fits snugly into the growing cup and has a tapered hole that forms a

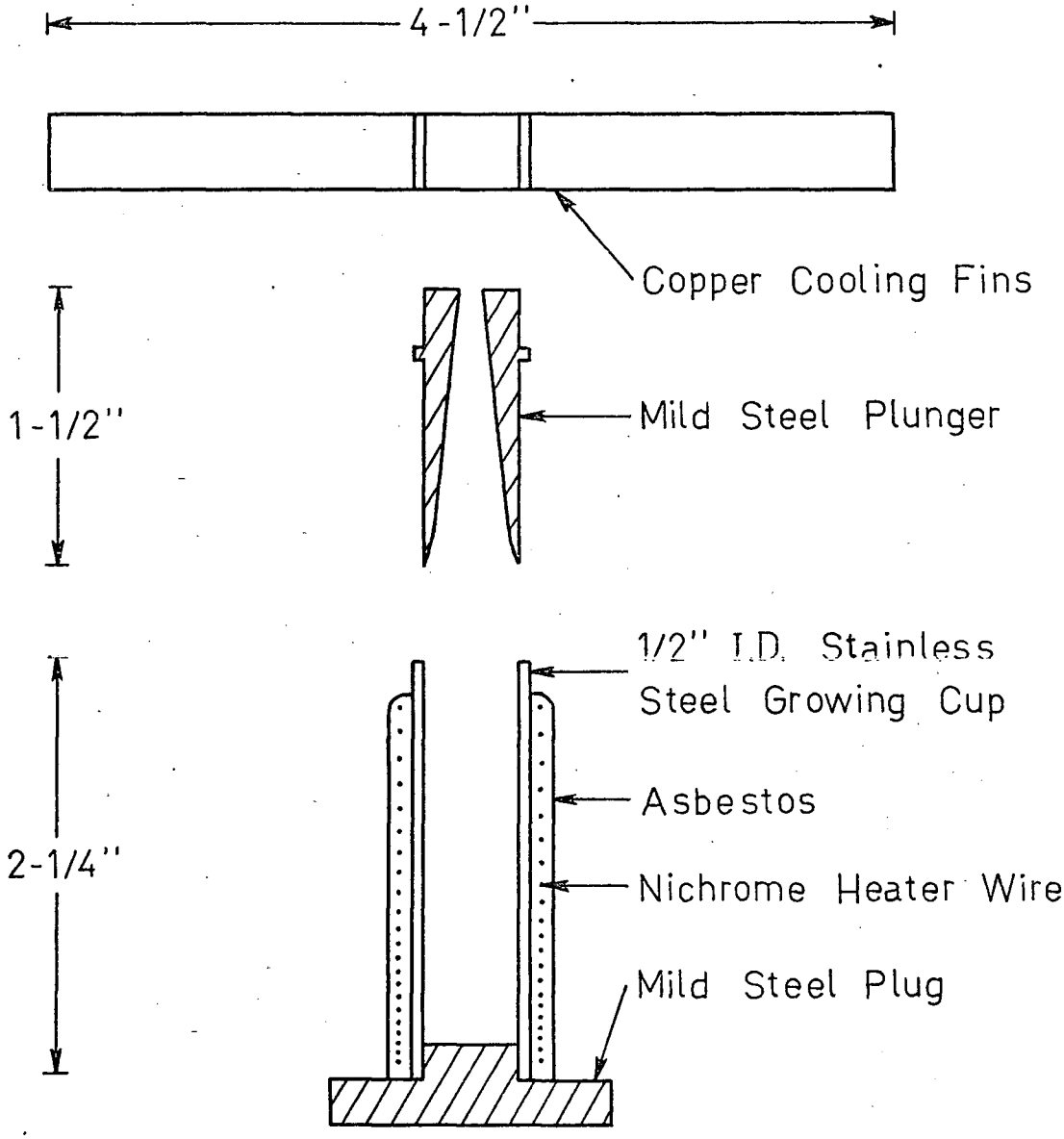

Figure 6: Cross-section of Crucible Used for Growing Lithium Single Crystals.

1/8 inch diameter nucleation tip at the top. Lastly, four copper cooling fins fit onto the top of the plunger to complete the effect of producing a high temperature gradient along the length of the crucible.

It is in the design of the plunger that this method differs from the standard Bridgman technique in which crystals are grown by cooling upwards from the bottom of the melt. Since molten lithium has a high surface tension and a low density (0.534 gm/cm^3 at 20°C and 0.498 gm/cm^3 at 300°C), the force of gravity will not cause it to flow into the apex of a small conical tip at the bottom of the melt. With the open tip design of figure 6, however, the molten lithium is forced up the central channel when the plunger is lowered into the crucible cup. Another advantage of cooling from the top of the melt is that impurities tend to settle downwards and spurious nucleations are limited to the small portion of the crystal which solidifies last.

Because lithium reacts with all known molecular gases at high temperatures, the entire growing process was carried out in a glove box filled with argon. A small quantity of phosphorus pentoxide was used to absorb water vapour since lithium at temperatures above its melting point (179°C) reacts rapidly in the presence of moisture to form a black hygroscopic nitride, Li_3N, which is easily distinguishable from the bright silver colour of the pure metal.

The actual procedure was as follows. Lithium rods 12.5 millimeters in diameter and 99.9% pure were purchased from Koch-Light Laboratories Limited. An ingot of proper size for the furnace was cut and scraped of its oxide layer before being placed into the growing cup. To retard chemical reactions and to facilitate removal from the crucible after cooling, the ingot and all surfaces touching it were coated with petroleum jelly. The lithium was then heated in the growing cup to approximately 320°C and stirred after 1-1/2 hours of heating. During this period the nucleation plunger was also preheated to the same temperature in a heater similar in design to the crucible containing the molten lithium.

After the heating period had passed, the surface of the melt was skimmed to remove the black nitride crust. Then the plunger was lowered into the crucible cup, forcing molten lithium up the central cone to form a nucleation bead at the top. The copper cooling fins were added and cooling was controlled manually with the variac at about 30 C°/hour until solidification was complete. The crystal was then removed from the mould and coated with petroleum jelly to protect it from oxidizing to a white powder during the process of orientation.

(ii) Crystal Orientation

Since lithium has a low electron density, Laue transmission patterns have usually been used to determine crystal orienta-

tion.[53,55,56,58] In a darkened room the Laue spots can actually be viewed directly on a fluorescent screen and compared with standard patterns for a body-centred cubic structure such as those given by Majima and Togino.[59]

Laue transmission photographs provided a rapid method of determining whether or not a particular sample was a good single crystal. The sample was mounted on a goniometer and translated so that its orientation with respect to the x-ray beam did not change. Using Polaroid Type 57 film, exposure times of only five minutes were required at settings of 12 keV and 20 ma. The primary beam easily passed through the entire two inch length of a sample, and if the patterns on successive photographs were invariant, it meant that a single crystal was present.

Feder[57] was able to obtain satisfactory back-reflection photographs of lithium crystals by using long exposure times, and since this method is more familiar it was used to determine the actual orientation of a sample. Settings of 10 keV, 30 ma, and 1-1/2 hours of exposure with wet process Ilford x-ray film resulted in the photographs shown in figure 7. Figure 7(a) is taken along the <001> crystallographic direction and figure 7(b) is within two degrees of the <011> direction. The Miller indices of the spots are given on the overlay. Since lithium crystallizes in the body-centred cubic structure, the only spots which occur are ones for which the sum of the indices is even.

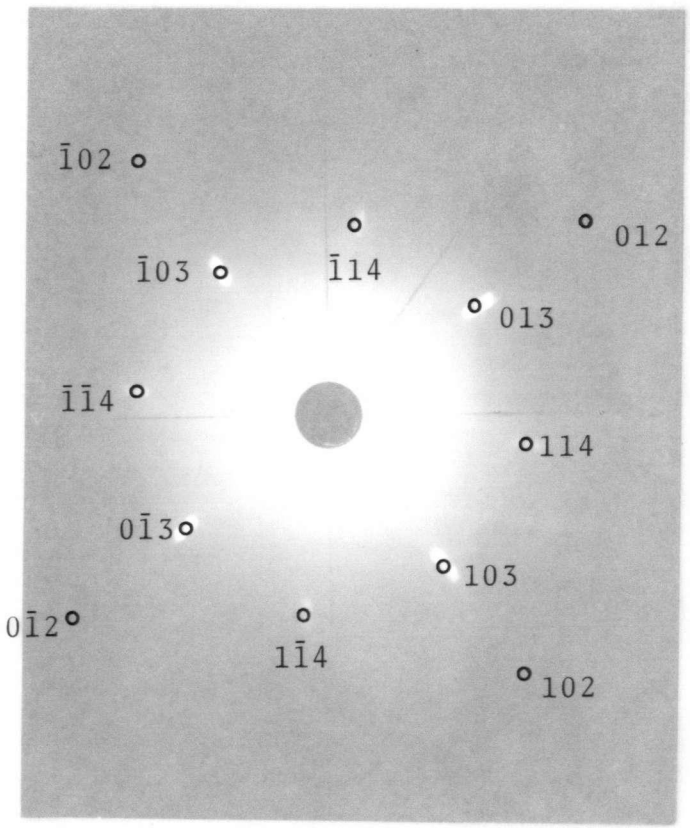

(a) Centred along the ⟨001⟩ crystallographic axis.

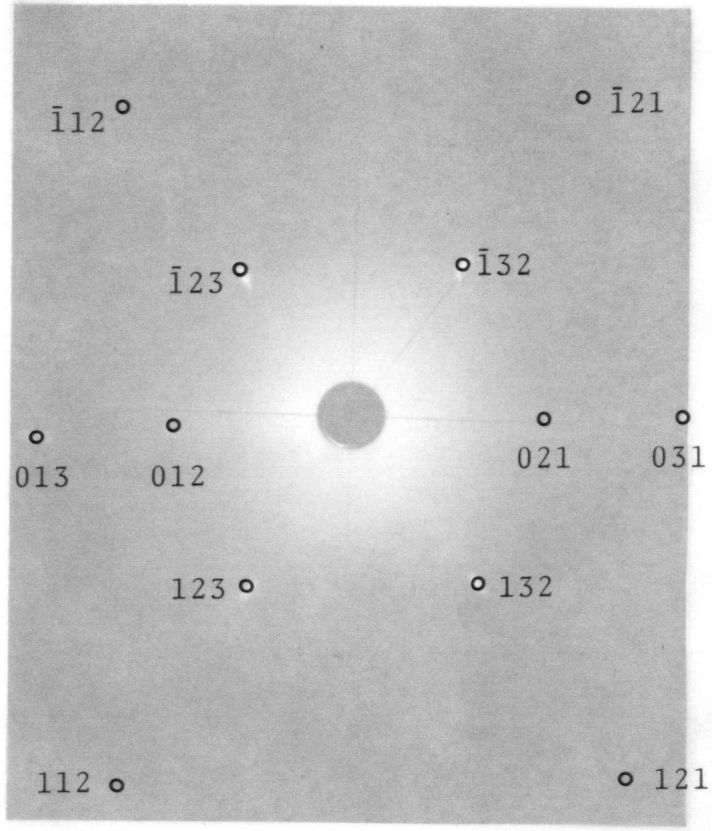

(b) Centred along the ⟨011⟩ crystallographic axis.

Figure 7: Laue back reflection photographs of a lithium single crystal.

(iii) Cutting and Etching

Once the crystallographic directions were determined, the crystal was attached to an aluminum block with GC Electronics 'Copper Print' and cut on an Agietron Spark Erosion Machine. This was modified so that the cutting edge was a travelling copper wire electrode 0.010 inch in diameter. For the soft alkali metals, Schiller et al.[60] have devised a rotating blade spark cutter which produces a better cut than either a stationary blade or a wire electrode. However, their method was not used since the small amount of surface damage produced by the wire electrode was easily removed during the etching process. Using the spark cutter at a working potential of 100 volts, a parallelpiped was cut with each face parallel to a (100) plane.

The crystal was then removed from the block and polished by lapping the surface against a piece of fine tissue which was laid on a glass plate and charged with methanol. An approximately cylindrical form was obtained by lapping four edges of the parallelpiped. This process must be carried out in air, and a mirror-like finish is obtainable by etching for a few seconds in methanol and then rinsing in xylene. Xylene also serves to remove the petroleum jelly coating which was necessary to protect the crystal during any long periods of exposure to air.

In its final form the sample was cylindrical, 3.5 millimeters in diameter and 4.5 millimeters in length, with the

<001> direction within three degrees of the cylinder axis. It was glued with 'Copper Print' to the end of a brass rod one inch in length and slightly smaller in diameter than the crystal itself. This rod served as a holder in the rotation experiment.

B The Positron Annihilation Facilities:

The apparatus for this study evolved from equipment used in previous investigations of copper and its alloys. Additional information to that provided here may be found in the graduate theses of Petijevich[61] and Becker.[62] The point geometry method described in Chapter II, section C(ii) is used, and provision is made for either a sideways motion of the detectors ($\theta \neq 0$) or a rotation of the specimen with the detectors fixed at $\theta = 0$.

The sequence of events in an experiment may be described with reference to figure 8 which shows the basic arrangement of the apparatus except for details in the vicinity of the source and sample. Positrons from the sodium-22 source are focussed onto the surface of the sample where annihilations with electrons produce gamma rays. A detector arrangment consisting of a NaI(Tl) scintillator crystal (Nuclear Enterprises Inc. type 408), and a photomultiplier tube (RCA-6342A or RCA-6810A), is placed behind a 4" thick lead block 25 feet away from the sample. The collimating hole in the lead block leading to the NaI(Tl) crystal is only 1/4 inch in diameter, therefore assuming that the sample is a point source, the

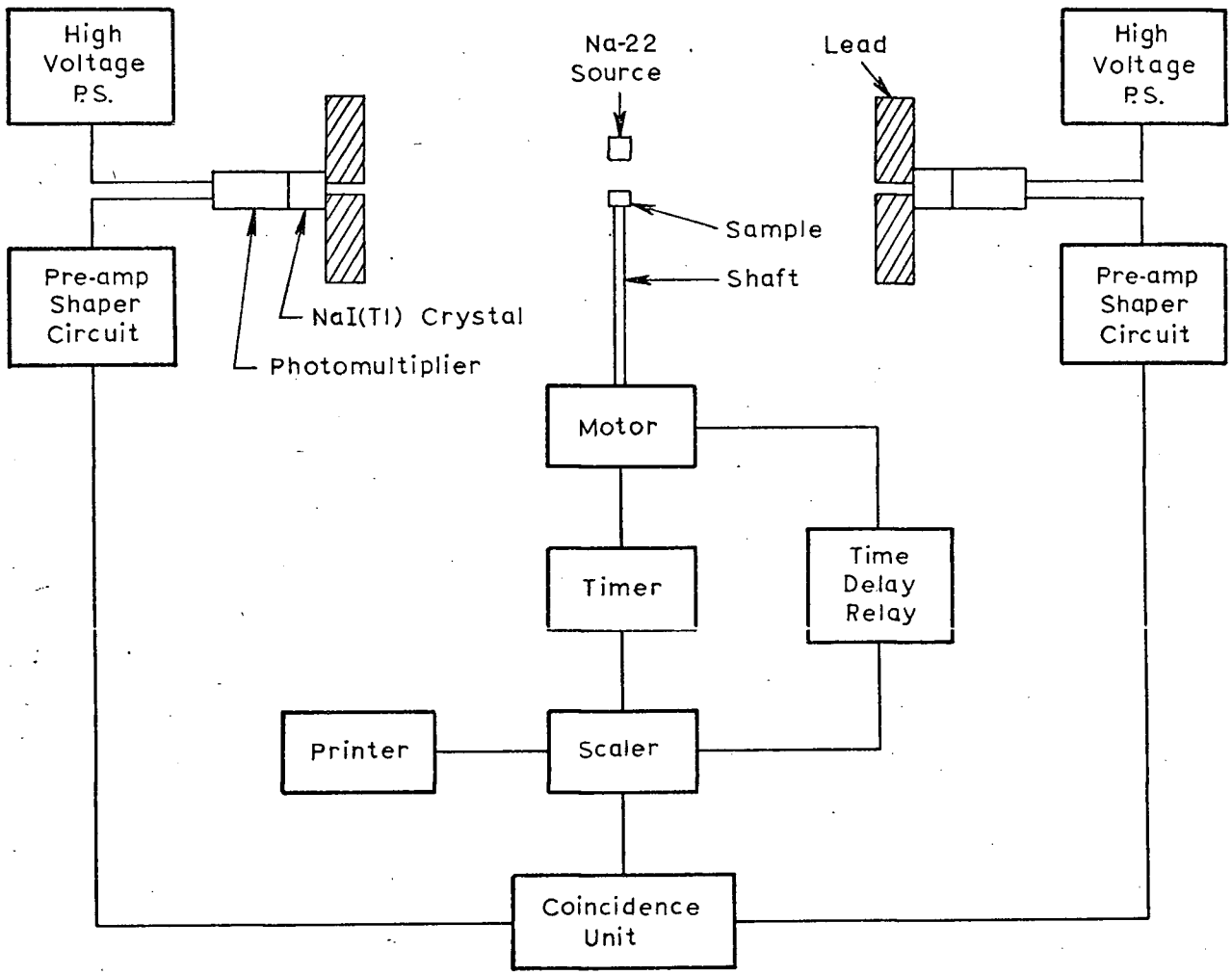

Figure 8: Block diagram of the experimental apparatus. Details in the vicinity of the sample are omitted.

geometric resolution is 0.8 milliradians. It has been determined (ref. 62, page 66) that the actual resolution function for this apparatus is approximately Gaussian, with a full width at half maximum of one milliradian.

When a gamma ray strikes a NaI(Tl) crystal, the light produced causes the photomultiplier tube to emit a pulse. This pulse is fed into a circuit which amplifies it to 1.5 volts and also shapes it into a form suitable for the fast coincidence circuit. A detailed schematic diagram of the pre-amplifier and shaper circuit is given in figure 9. This circuit also serves as an energy discriminator so that all pulses below 140 keV are eliminated.

Pulses from a pair of detectors which are aligned collinearly with the crystal at $\theta=0$ are fed into the fast coincidence circuit of figure 10. If two pulses from the pair of detectors arrive at the inputs within 25 nanoseconds, their combined voltage of 3 volts is sufficient to fire the tunnel diode. This, in turn, switches on the three transistors in the circuit and a single coincidence count is registered on a Canberra Industries model 1473 scaler.

The resolving time, τ, of each coincidence circuit is measured using a random source method. If N_1 and N_2 are the counts produced in two detectors by uncorrelated sources, the number of chance coincidences recorded is given by

$$N_{chance} = 2\tau N_1 N_2 .$$

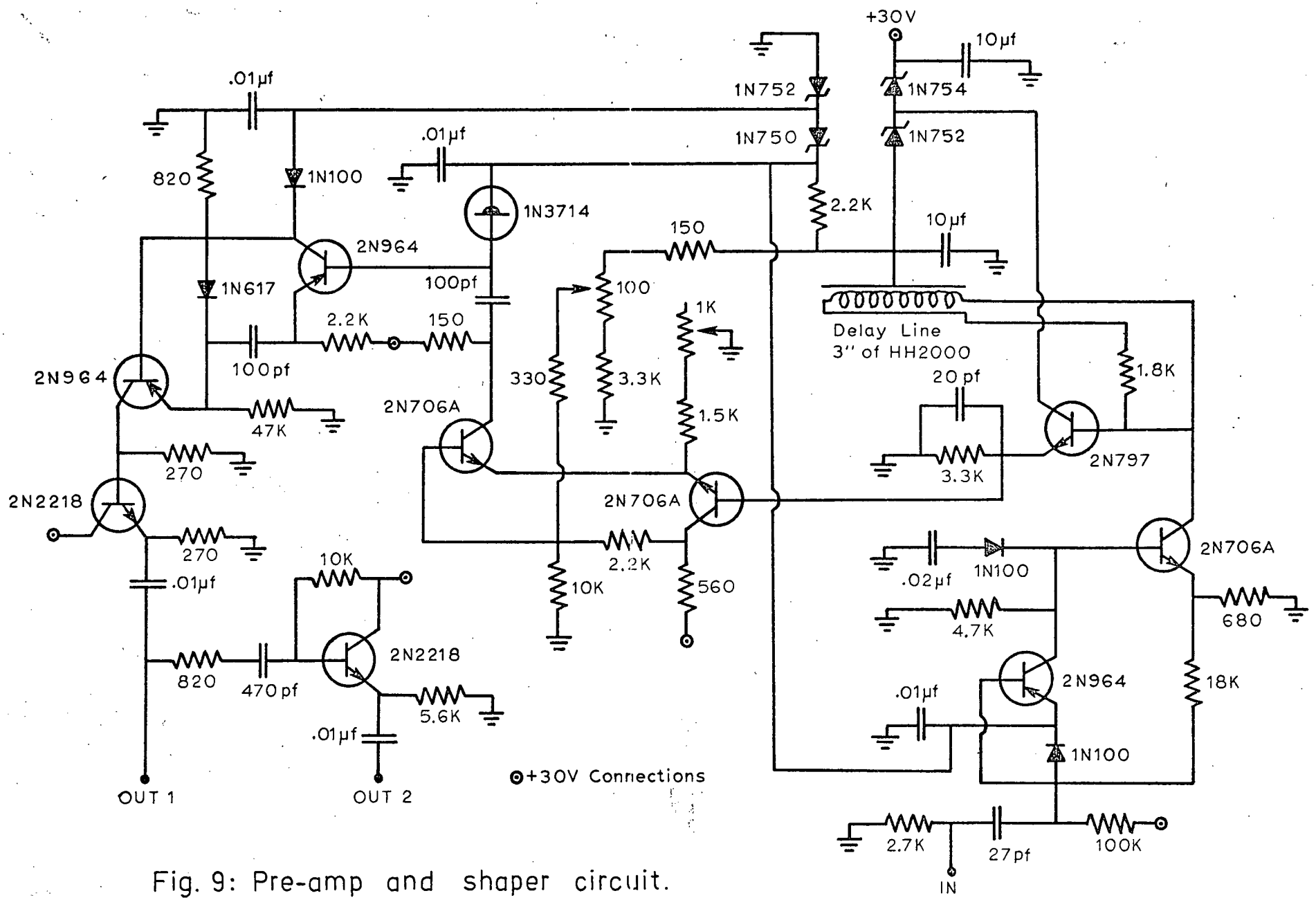

Fig. 9: Pre-amp and shaper circuit.

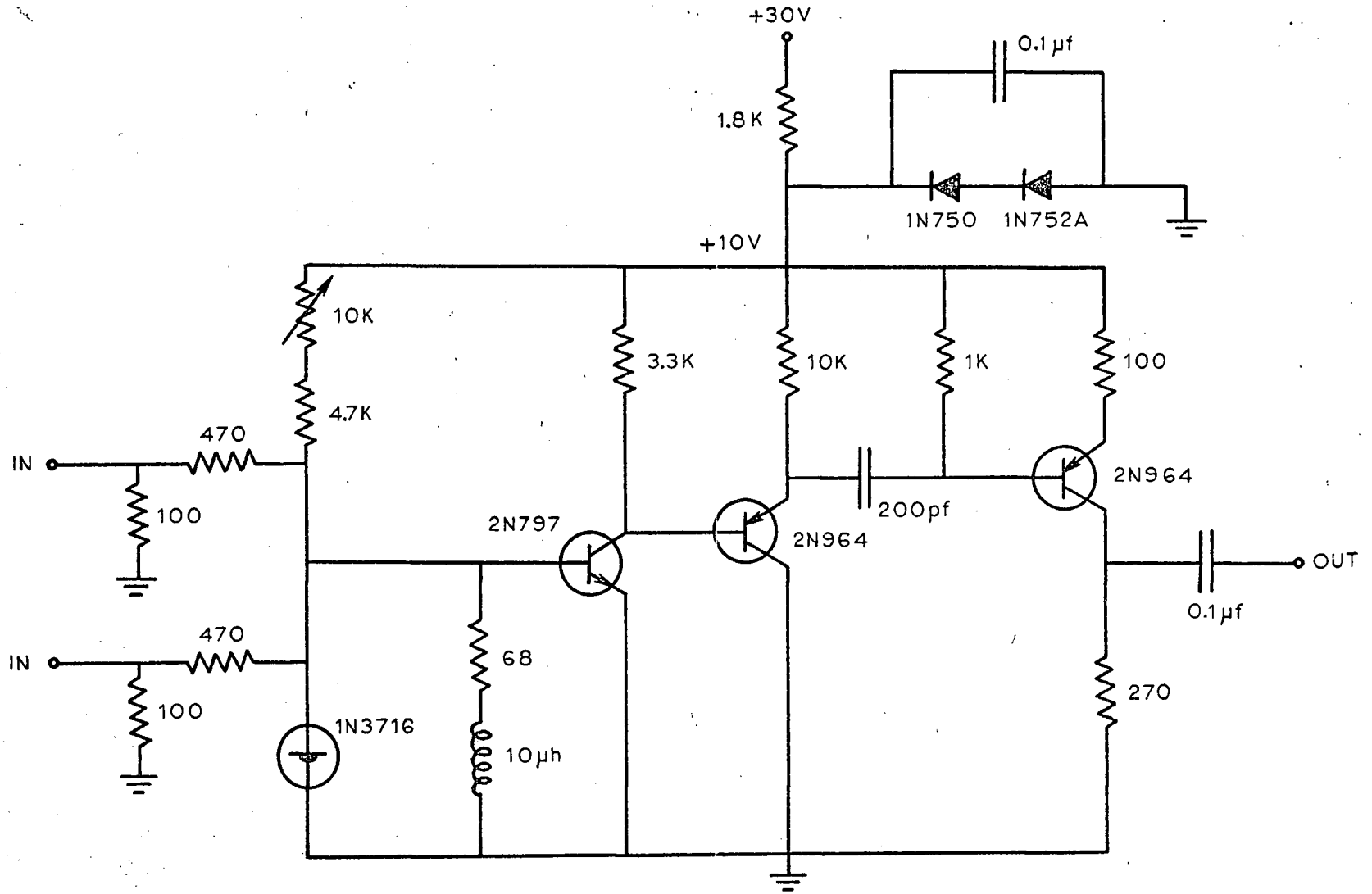

Figure 10: Coincidence circuit.

By adjusting the potentiometer which controls the bias on the tunnel diode in figure 10, the resolving time, τ, can be adjusted to approximately 25 nanoseconds. To obtain the maximum coincidence count rate, the cable lengths from the detectors to the coincidence circuits must also be optimized so that the time required for a pulse to reach the coincidence circuit is the same for each detector in a pair.

For an experiment in which the crystal is rotated, the sample holder fits into the end of a hollow shaft which leads to the rotation motor. In order to stop the rotation only in particular directions, a 12 inch diameter brass disc which has notches on the circumference (in this case at 45° intervals) is mounted on the shaft of the motor. When the motor is turned from one position to the next, a microswitch riding the circumference of the wheel immediately stops the rotation when the succeeding notch is reached.

To prevent such factors as source decay and drifts in the electronics from introducing anisotropies in the experimental result, it is desirable to count in one particular orientation only for a relatively short time compared with the time required for the entire experiment. A Canberra model 1492 timer was used to control this interval. After counts had been accumulated for twenty minutes in one position, a pulse from the timer activated a Canberra model 1489 tape printer which printed out the number of coincidence counts registered on each scaler.

At the same time, the motor rotated the specimen to the next position on the wheel. While the motor turned and the number of counts was being printed, a time delay relay inactivated the scalers so that no false counts could be registered. The scalers then began counting from zero in the new position and the above procedure was repeated automatically until a sufficient number of counts for good statistics was accumulated.

Figure 11 gives a more detailed view of the apparatus in the vicinity of the sample. Since approximately one half of the positrons striking the sample are absorbed within 0.04" (ref. 2, page 81), it was necessary to enclose the sample in a helium atmosphere to minimize oxidation of the surface. Alternatively, the chamber could have been evacuated, but this would have little advantage because the penetration depth of positrons in helium is large. This was confirmed by the very low background count obtained when the sample was removed. The helium atmosphere was contained in an airtight brass box of dimensions 3" × 6" × 6" placed between the pole faces of the magnet used to focus the positrons onto the sample. Approximately every eight hours, the box was flushed with helium through a valve and outlet (not shown) located on the top and bottom of the box respectively. The annihilation photons escaped to the detectors through clear lucite windows on the sides of the box.

The positrons were emitted from a sodium-22 source pur-

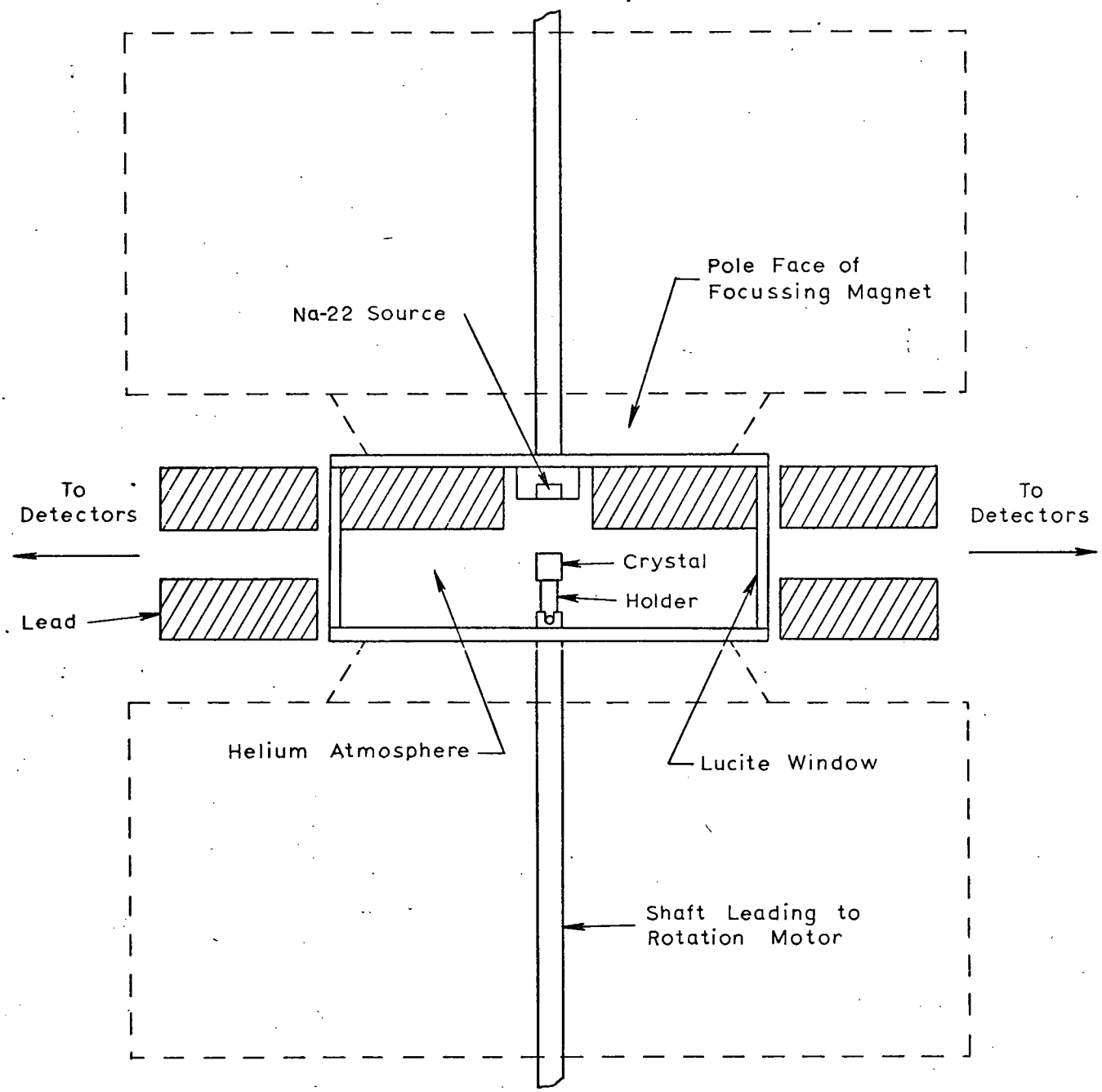

Figure 11: Top view of details of the apparatus around the sample.

chased from New England Nuclear Corporation. Its initial positron activity at the time of purchase was 30 millicuries, but because the half-life of sodium-22 is 2.6 years, the strength at the time of this experiment was about 10 millicuries. A strong magnetic field was used to focus the positrons onto the surface of the sample, and lead blocks were arranged as shown in figure 11 so that the detectors could not register annihilations from the source, sample holder, or sides of the box.

In order to prevent the time required to perform an experiment from becoming prohibitive, it was necessary to have six separate pairs of detectors accumulating counts. Each pair is connected to a separate coincidence circuit so that no cross correlations can occur, and the outputs from two coincidence circuits are fed into one of three separate scalers. Obviously, since each pair of detectors cannot occupy the same position in space, the cylinders through $\underline{k}$-space [see fig. 3(b)] will not be parallel to each other. However, since the sample to detector distance is large, no detector is more than 2° from the true direction of interest at $\theta=0$. The resolution function of 0.8 milliradian subtends a much larger angle at the Fermi radius (approximately 21.5° in the case of lithium), hence the error introduced is not significant.

At the start of an experiment, the detectors and sample are aligned in the $\theta=0$ position so that a single pair of

detectors passes collinearly through the surface of the sample. This alignment is performed optically using a surveyor's level to measure the vertical height of the detectors, and a transit to measure the horizontal positions. The accuracy of this alignment is approximately ±0.05 millimetres over the entire distance of 20 metres between the detectors.

CHAPTER IV

ANALYSIS OF DATA

A Experimental Results:

Of the several possible rotations of interest in a body-centred cubic crystal, the most statistically favourable one for comparing the <110> and <100> directions is a basal plane rotation in which the axis of rotation is along the <001> crystallographic direction. If this axis is perpendicular to the line joining the detectors, then a single rotation will expose the <100>, <110>, <010>, $<\bar{1}10>$, $<\bar{1}00>$, $<\bar{1}\bar{1}0>$, $<0\bar{1}0>$, and $<1\bar{1}0>$ directions respectively. Since each of these directions is separated by 45°, it was necessary to construct the rotation control wheel with eight notches along the circumference. These notches were numbered 1 to 8, and the crystal was oriented so that an odd position corresponded to a <110> direction and an even position corresponded to a <100> direction.

In addition to the fact that each of the above principal directions occurs an equivalent of four times in 360°, the basal plane rotation has the advantage that the directions exactly between the principal directions are all equivalent. These midpositions do not correspond to directions with low Miller indices, but they lie within a degree of the <520> direction. If the crystal is rotated by 22.5° with respect to

the wheel, it is apparent that the coincidence count rate in each position should be the same. This serves as a useful check that any anisotropy observed in comparing the <110> and <100> directions is genuine.

Even with six pairs of detectors, the total count rate was only about 4.5 counts each minute, and to obtain good statistics it was necessary to count for a total of 16 days. Two thirds of this time was devoted to sampling the <110> and <100> directions, and one third was devoted to the midposition. As stated previously, the wheel remained at one particular notch for only twenty minutes before being rotated to the next position. To ensure that the total counts for the midposition could be normalized to the other two directions, counting was carried out in the principal directions for two days and then the sample was rotated by 22.5° to the midposition for one day. This process was repeated until the experiment was completed.

Finally, a background count was taken for a period of 4.7 days. This was accomplished by removing the sample and holder but leaving the rest of the experimental apparatus exactly as before. The background count which is measured in this way arises from annihilations in the helium and the sides of the box used to contain it. There are also a small number of chance coincidences from power line fluctuations, cosmic rays, and other detector noise. The number of counts recorded amounted to approximately 2% of the total coincidence counts.

Figure 12 displays the experimental results after the background has been subtracted. No correction has been applied for the decay of the sodium-22 source since its half-life is 2.6 years and the slow decay will be averaged out by the rotation.

Each graph in figure 12 represents the output from a single scaler or two pairs of detectors. The graphs on the left correspond to the principal directions, with the <110> directions in the odd numbered positions and the <100> directions in the even numbered positions. The right-hand graph of each pair corresponds to the midposition results for the same detectors as on the left. The error bar on each experimental point represents $(\sqrt{N_c} + \sqrt{N_b})$, where N_c is the total number of coincidence counts registered and N_b is the corresponding number of background counts.

An examination of the graphs on the left shows that the <110> points are all higher than the <100> points except for positions 4 and 5 in the middle and bottom rows. In contrast, the midposition graphs do not appear to exhibit any definite order.

These trends are illustrated more clearly in figure 13 which is an accumulation of the results in figure 12. The top graph indicates a significant increase in the number of counts for the <110> directions, whereas in the bottom graph the effect is markedly reduced. If the odd positions in the bottom graph are considered separately from the even positions, the actual

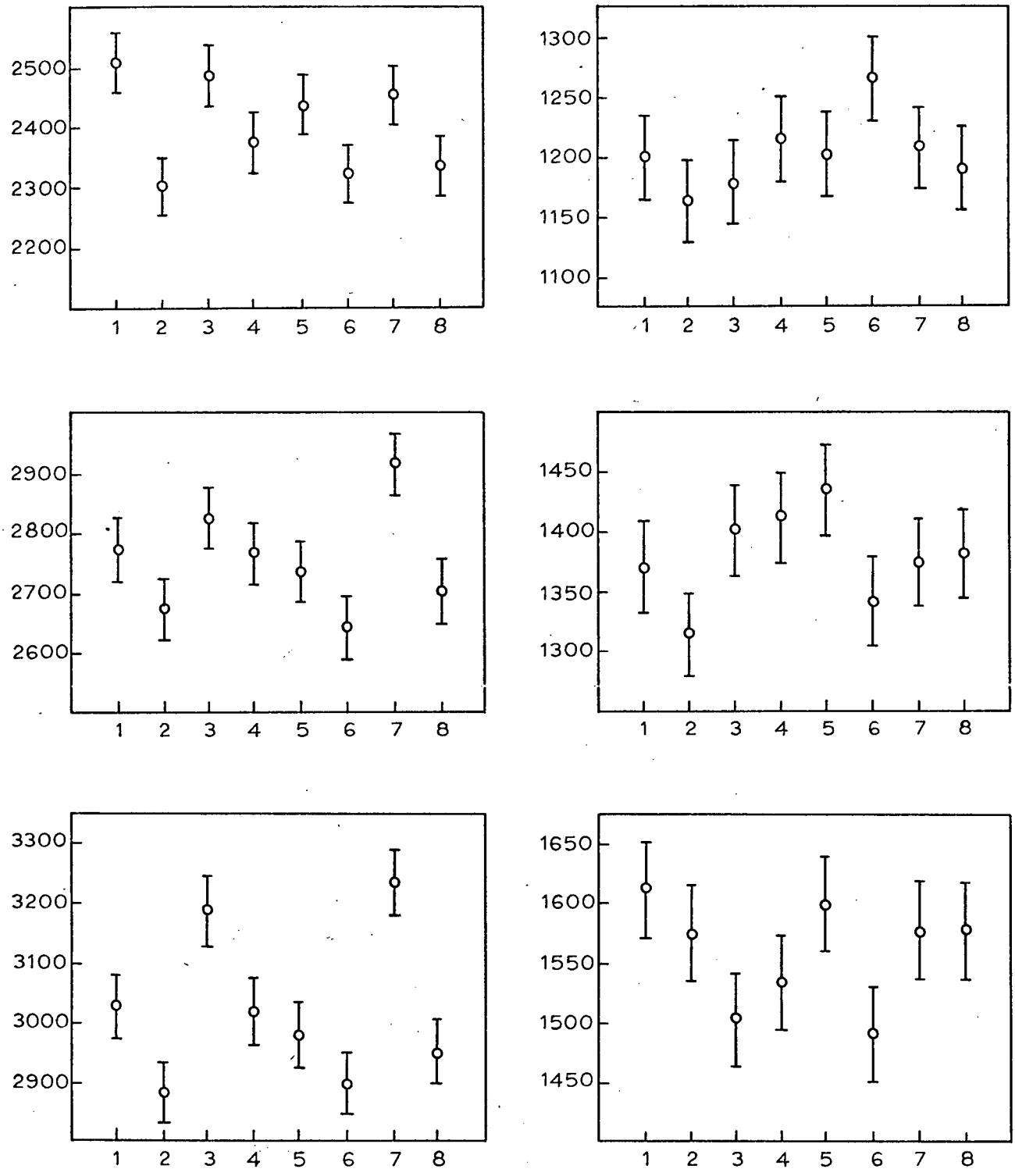

Figure 12: Experimental results. Coincidence counts versus wheel position. On the left-hand graphs, odd positions are ⟨110⟩ directions and even positions are ⟨100⟩ directions. The right-hand graphs are the midposition results for the same detectors as on the left. Each graph represents the counts from two pairs of detectors.

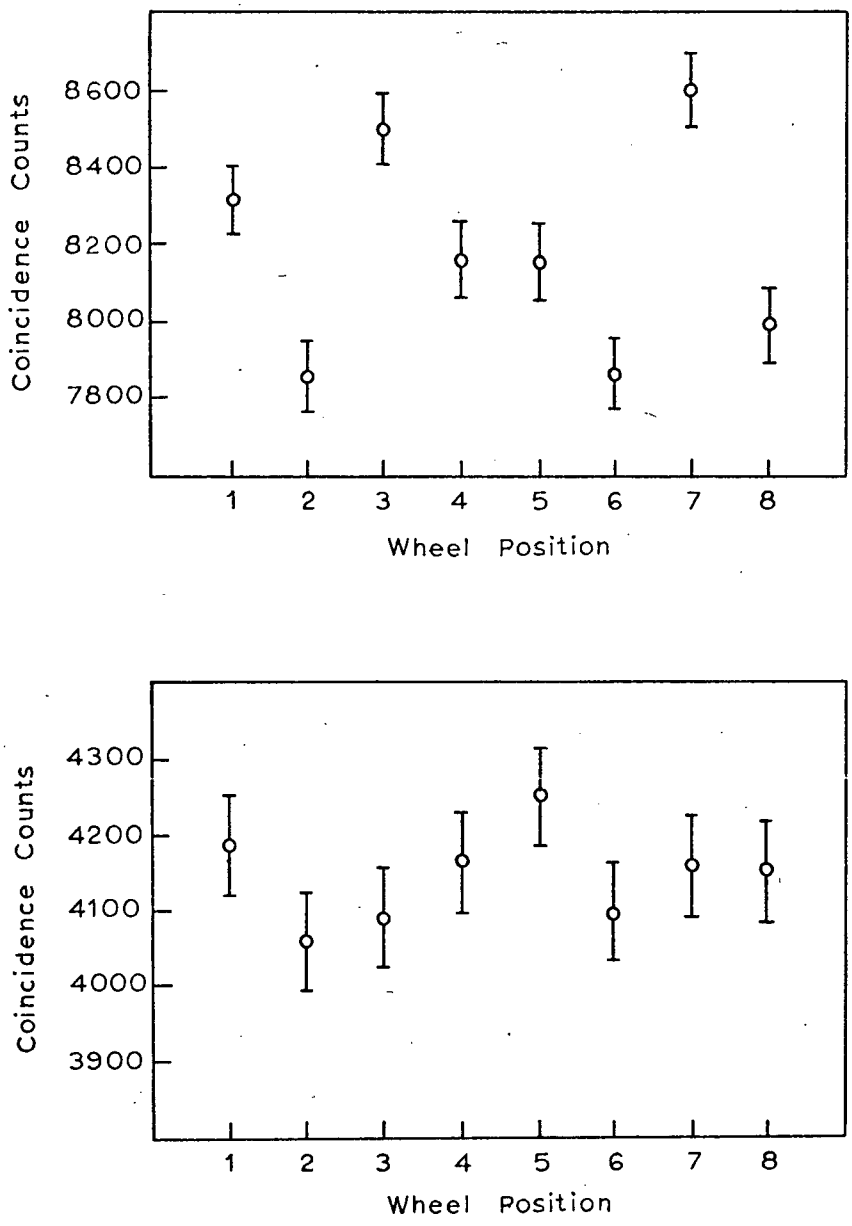

Figure 13: Cumulative results from fig. 12. The top graph gives the ⟨110⟩ and ⟨100⟩ directions (odd and even positions respectively). The bottom graph gives the midposition result.

numerical values are 16,679 ± 147 and 16,468 ± 146 respectively. Although the odd position count is 1.3% higher than the even position count, the difference is within the statistical error as would be expected for equivalent points.

The data of figures 12 and 13 can be reduced further to give the number of counts registered in each of the three different directions sampled by this experiment. The numerical results are given in table 2; the four rows of the table corresponding to the four pairs of graphs given in figures 12 and 13. The midposition is automatically normalized to the other two directions because of the manner in which the experimental data was accumulated.

Comparing the <110> and <100> directions of each row of table 2, it is found that the <110> direction is respectively 5.9%, 4.4%, 5.6%, and 5.3% greater than the <100> direction. The net difference of 5.3% is obviously significant compared with the errors of ±0.6% on each of the two points. This result agrees well with the one obtained from the phenomenological model of Donaghy and Stewart.

The midposition count in table 2 occurs midway between the principal direction counts in the first two rows, but is higher than the <110> count in the third row. The net result is that the midposition total is 4% higher than the <100> total. According to the results of Donaghy and Stewart (ref. 4, page 395, figure 5), the midposition should not be more than 1% higher

Table 2

A comparison of the numerical values of the coinci counts for the 3 different directions. The first 3 row the table correspond to the 3 pairs of graphs in figure and the last row corresponds to the accumulated results in figure 13.

	<110>	Midposition	<100
1	9885 ± 114	9629 ± 113	9337 ±
2	11,253 ± 123	11,046 ± 122	10,782 ±
3	12,424 ± 126	12,472 ± 127	11,762 ±
4	33,562 ± 210	33,147 ± 202	31,881

than the <100> direction. The fact that the result here is significantly greater does not constitute a serious discrepancy between these two experiments. There are two reasons for this. Firstly, it can be estimated that the full width at half maximum of the resolution function in this experiment subtends an angle of 21.5° at the Fermi radius (ref. 62, page 66). If this resolution function overlaps the side of the bulge in the <110> direction, the count rate in the midposition will be artificially enhanced. Secondly, it will be shown later that the higher momentum components of the electron wavefunction can have a significant effect on the count rate, and this effect is not easy to determine for the midposition. For these reasons the usefulness of the midposition result is limited to verifying that the count rate is isotropic for equivalent crystallographic directions.

B Higher Momentum Components of the Positron Wavefunction:

A detailed examination of the higher momentum components of the electron and positron wavefunctions is necessary in order to determine whether or not the observed 5.3% difference between k_{110} and k_{100} arises from a genuine distortion of the Fermi surface of lithium. If these higher momentum components are large, the nearly free electron approximation is obviously inapplicable. Even when they are relatively small, however, the higher momentum components have an important experimental

significance since they determine the number of states $\underline{k}$ which are scattered by a reciprocal lattice vector. Such states are not detected because they generally lie outside the experimental resolution function.

In equation (2) on page 8, it was assumed that the positron wavefunction $\phi_+(\underline{r})$ could be considered constant. The validity of this assumption can be examined by expanding the wavefunction of a thermalized ($\underline{k}$=0) positron in a series involving reciprocal lattice vectors $\underline{K}$:

$$\phi_+(\underline{r}) = a_o + \sum_{\underline{K}} a_{\underline{K}} e^{i\underline{K}\cdot\underline{r}} . \qquad (9)$$

If the coefficients $a_{\underline{K}}$ are small, their values are given from first order perturbation theory by

$$a_{\underline{K}} = \frac{V_{\underline{K}}}{\frac{\hbar^2 K^2}{2m}} \qquad (10)$$

A value for a_o must be determined from the normalization condition $|a_o|^2 + |a_{\underline{K}}|^2 = 1$. The Fourier coefficients, $V_{\underline{K}}$, of the potential seen by the positron may be calculated by a direct method developed by Stroud and Ehrenreich.[18] By utilizing the relationship between the electron charge density and the x-ray form factor, the Fourier coefficients can be obtained directly from experiment without the necessity of having to choose a particular form for the potential. The detailed application of this procedure to lithium is given in Appendix I.

For the two shortest reciprocal lattice vectors $K_{110} = 2\sqrt{2}\pi/a$ and $K_{200} = 4\pi/a$, the values of the Fourier coefficients are $V_{110} = 0.1182$ Ry. and $V_{200} = 0.0713$ Ry. Atomic units (see page 27) are used to simplify the calculations. In these units equation (10) becomes

$$a_{\underline{K}} = \frac{V_{\underline{K}}}{K^2} \qquad (11)$$

and the coefficients are

$$a_{110} = 0.0636 \qquad \text{and} \qquad a_{200} = 0.0192$$

for a lattice constant of $a = 6.5183$ a.u. Considering the fact that twelve (110) and six (200) planes contribute to the scattering, the probabilities of interest are:

$$|a_o|^2 \simeq 0.95$$
$$12|a_{110}|^2 = 0.0486$$
$$6|a_{200}|^2 = 0.0022$$

It is obvious from these values that the first coefficient is dominant and the procedure of terminating equation (9) after a_o is justified.

The above result is consistent with the results of other authors[16,63] who have chosen a form for the potential and then calculated positron wavefunctions in the Wigner-Seitz approximation which requires spherical symmetry and zero slope at the Wigner-Seitz radius.

C Higher Momentum Components of the Electron Wavefunction:

The task of evaluating the higher momentum components of the electron wavefunction is not as straightforward as it was for the positron. In the nearly free electron approximation, the conduction electron wavefunction can be expanded as

$$\psi(\underline{k},\underline{r}) = \sum_{\underline{K}} a_{\underline{K}}(\underline{k})\ e^{i(\underline{K}-\underline{k})\cdot\underline{r}}\ , \tag{12}$$

where the coefficients can be obtained from first order perturbation theory as before:

$$a_{\underline{K}}(\underline{k}) = \frac{V_{\underline{K}}}{E_{\underline{K}-\underline{k}} - E_{\underline{k}}}\ . \tag{13}$$

The difficulty is that no direct method is available for obtaining the Fourier coefficients of the potential, and if one assumes a form for the potential then one effectively assumes a shape for the Fermi surface. Thus, the procedure of adopting a potential to determine the effect of the higher momentum components of the electron wavefunction is inconsistent. Nevertheless, since the Fermi surface of lithium is not greatly distorted and the theoretical calculations appear to be relatively insensitive to small differences in the potential, it is hoped that such a procedure will allow a reasonable estimate of the higher momentum components to be made. The first five values of $V_{\underline{K}}$ for a flattened Seitz potential are given in table 3 as taken from the paper of Schlosser and Marcus.[28] These

Table 3

Fourier coefficients of lithium for a flattened Seitz potential (taken from Schlosser & Marcus[28]). The lattice constant is a=6.5183 a.u.

$\underline{K}$	$\lvert\underline{K}\rvert$	$-V_{\underline{K}}$
0	0.0000 a.u.	1.00221 Ry.
110	1.3632	0.16889
200	1.9279	0.09435
211	2.3611	0.06388
220	2.7264	0.05166

coefficients are very similar to those obtained from the OPW method of Callaway.[32,33]

As indicated previously, the quantity $|a_{\underline{K}}|^2$ determines the probability that a photon pair will have momentum $\hbar(\underline{K}-\underline{k})$. Hence, these coefficients will determine the number of pairs that are not detected, and it is necessary to compare their effect on the count rate along the <110> and <100> directions.

The number of counts lost along the <100> direction will be considered first. Figure 14(a) shows a cross section through the first Brillouin zone and free electron sphere in $\underline{k}$-space, with the slice being taken parallel to the basal plane. It will be helpful throughout this discussion to refer to the diagram of the first Brillouin zone of lithium given on page 25. The actual width of the resolution function along the <100> direction is shown by the dotted lines in figure 14(a). For convenience it will be assumed that this resolution is actually a line through $\underline{k}$-space, although this will obviously limit the validity of the result obtained.

Considering the state $\underline{k}$ and the state scattered by the (110) plane 'B' in figure 14(a), it is possible to express the energies required in the denominator of equation (13) as

$$E_{\underline{k}} = \frac{\hbar^2}{2m}\left(k_x^2 + k_y^2\right)$$

and $$E_{\underline{K}-\underline{k}} = \frac{\hbar^2}{2m}\left((K-k_x)^2 + k_y^2\right) .$$

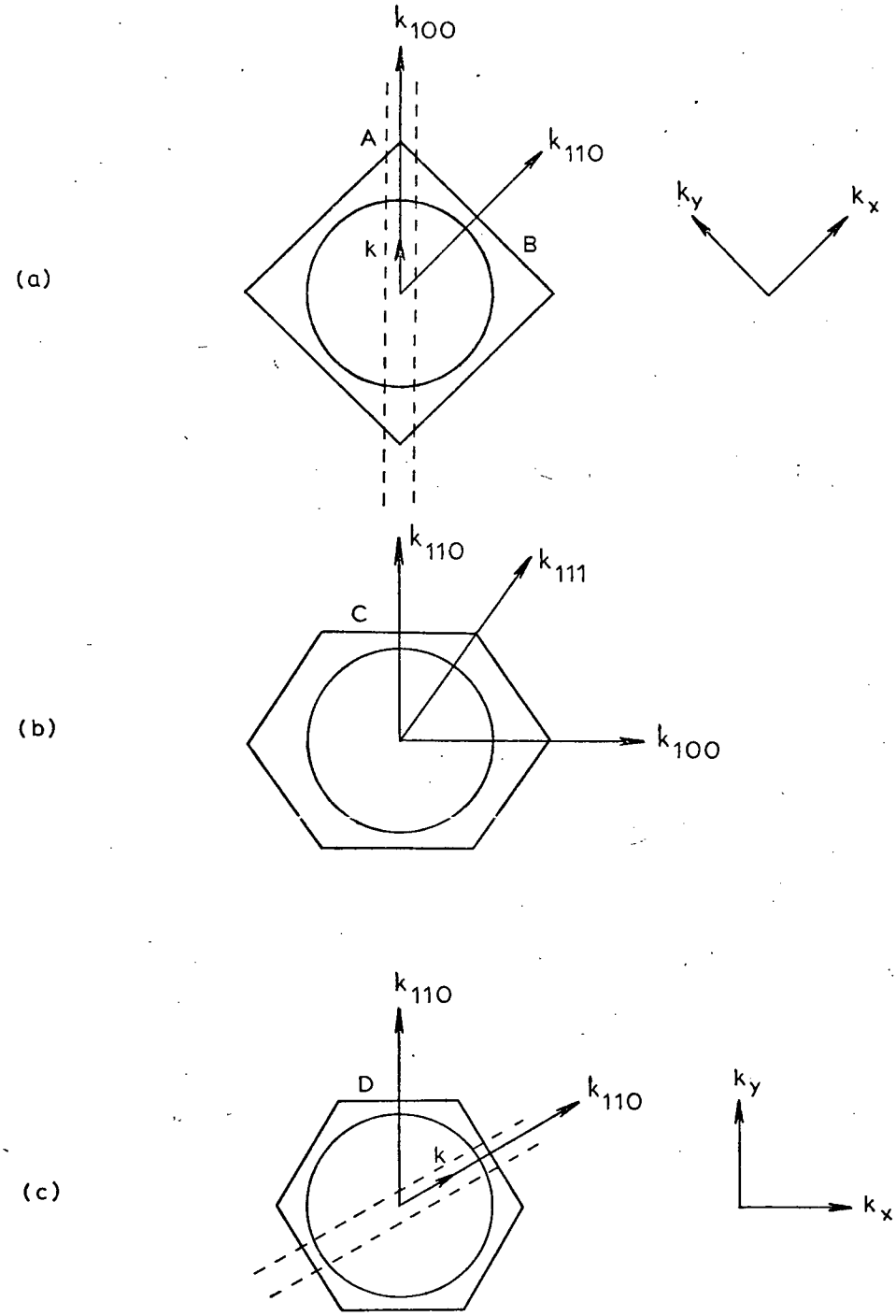

Figure 14: Cross-sections through the first Brillouin zone of lithium.

The co-ordinate axes are taken as shown in the diagram. Hence,

$$E_{\underline{K}-\underline{k}} - E_{\underline{k}} = \frac{\hbar^2 K^2}{2m}\left(1 - 2k_x/K\right)$$

and since $k_x = k \sin 45°$, it is possible to write equation (13) for the coefficients in atomic units as

$$a_{\underline{K}} = \frac{V_{\underline{K}}}{K^2\left(1 - \sqrt{2}k/K\right)} . \qquad (14)$$

As expected, the magnitude of $a_{\underline{K}}$ depends on the distance from the zone boundary. The coefficient necessary for the explicit calculation is V_{110} in table 3, and values of $|a_{\underline{K}}|^2$ for selected distances from $-k_F$ to k_F are given in column A of table 4. These coefficients are evidently much larger than the coefficients of the positron wavefunction. An average value of $|a_{\underline{K}}|^2$ for column A is easily obtained from the usual relation

$$\overline{|a_{\underline{K}}|^2} = \frac{\int_{-k_F}^{k_F} |a_{\underline{K}}|^2 \, dk}{\int_{-k_F}^{k_F} dk} .$$

This yields $\overline{|a_{\underline{K}}|^2} = 0.01316$ for the single plane 'B' in figure 14(a). However, four such planes of the Brillouin zone come together at 'A' to form the corner, and since there are four on the other side of the zone it is necessary to multiply $\overline{|a_{\underline{K}}|^2}$

Table 4

Fraction of k_F	Column A $\lvert a_{\underline{K}} \rvert^2$	Column B $\lvert a_{\underline{K}} \rvert^2$
1.0	0.0543	0.0255
0.8	0.0315	0.0193
0.6	0.0205	0.0150
0.4	0.0145	0.0121
0.2	0.0107	0.0099
0.0	0.0083	0.0083
-0.2	0.0066	0.0070
-0.4	0.0053	0.0060
-0.6	0.0044	0.0052
-0.8	0.0037	0.0046
-1.0	0.0032	0.0040
Average	0.01316	0.01015

Column A gives the values of $\lvert a_{\underline{K}} \rvert^2$ for the scattering of a state $\underline{k}$ by the plane 'B' in figure 14(a).

Column B gives the values of $\lvert a_{\underline{K}} \rvert^2$ for the scattering of a state $\underline{k}$ by the plane 'D' in figure 14(c).

by eight to obtain a total contribution of 0.105 from these planes. Finally, it can be shown that the other four planes of the Brillouin zone are of the type 'C' shown in figure 14(b). Since these are all parallel to the <100> direction, each will have $|a_{\underline{K}}|^2 = 0.0083$ from table 4. Adding the contributions from all twelve (110) planes, the result is 0.138.

It is apparent that four of the six (200) planes will also affect the count rate, although scattering from these planes is reduced because of the smaller value of V_{200} and the larger value of K_{200}. The net effect of these planes is to reduce the count rate by 0.3%. Hence, the effect of scattering from both the (110) and (200) planes implies that a total of 14.1% of the annihilation pairs will not be detected when the apparatus is aligned along the <100> direction.

Now consider the number of counts lost when the apparatus is aligned along the <110> direction. From figure 14(a) the scattering from the two planes equivalent to 'B' will be counted except for a few states which lie outside the resolution function. The other two planes will contribute 0.0083 each, or a total of 1.7%.

The remaining eight planes are all of the type 'D' shown in figure 14(c), where the resolution function is along the direction shown. Choosing the co-ordinate axes as indicated, it is possible to calculate an expression for the coefficients similar to equation (14). In this case, however, $k_y = k \cos 60°$

and the result is

$$a_{\underline{K}} = \frac{V_{\underline{K}}}{K^2(1 - k/K)} . \qquad (15)$$

The required Fourier coefficient is once again V_{110}. Values of $|a_{\underline{K}}|^2$ for points from $-k_F$ to $+k_F$ are given in column B of table 4. As expected, their initial value at k_F is lower than for column A, but they do not diminish as rapidly. The average value can be calculated as before and is equal to 0.01015. For the eight planes of this type the contribution is 8.1%, hence the total number of counts lost along the <110> direction from scattering by the (110) planes is 9.8%. A consideration of the effect of the (200) planes raises this value to 10.2%.

If the losses of 10.2% and 14.1% for the <110> and <100> directions are corrected for in the experimental data given on page 59, the resulting totals are 36,985 and 36,376 respectively. The true distortion in the Fermi surface would then be reduced to 1.7% which is not appreciably greater than the statistical accuracy.

The above calculation reveals that the higher momentum components of the electron wavefunction have a significant effect on the observed anisotropy. The indication is that the 5.3% difference between the number of counts in the <110> and <100> directions should be regarded as an upper limit to the true distortion of the Fermi surface.

A more thorough examination of the effect of the higher momentum components of the wavefunctions is obviously desirable. A complete calculation would have to consider higher terms in the electron and positron expansions, as well as the effect of the broad experimental resolution function. In addition, it would be necessary to examine the effect of the choice of the potential, since the adoption of particular values for the Fourier coefficients is the most significant assumption made in this analysis.

D Enhancement and Annihilations with Core Electrons:

Melngailis and DeBenedetti[16] have found that better quantitative agreement is obtainable if Kahana's enhancement factor is included in calculating the angular correlation curves of Donaghy and Stewart from OPW wavefunctions. The enhancement factor has been considered isotropic in this analysis. Its omission should not be serious because the Fermi surface of lithium is nearly spherical and any effect would certainly be weaker than the effect of the higher momentum components of the electron wavefunction. In addition, an examination of figure 8 on page 405 of Melngailis and DeBenedetti's paper shows that enhancement does not affect the shape of the distribution near $\theta=0$.

The last effect which must be considered is that of annihilation with core electrons. From the considerations of Melngailis and DeBenedetti, this contribution is an order of magnitude smaller than the contribution from conduction electrons for the long slit geometry. Since the point geometry arrangement samples an even smaller proportion of the core electrons relative to the conduction electrons in $\underline{k}$-space, it can be calculated that approximately 5% of the coincidence counts arise from annihilations with core states. This small isotropic contribution can be subtracted, with the result that the total anisotropy between the principal directions increases to 5.6%.

CHAPTER V

CONCLUSIONS

This chapter presents a brief summary of the results of this experiment. The main feature is that the number of counts in the <110> direction is found to be 5.3 ± 1.2 percent greater than the number in the <100> direction. This anisotropy is increased to 5.6% if the contribution from annihilations with core electrons is subtracted from the total number of counts.

Since the collinear point geometry is used, the evidence that the Fermi surface of lithium is distorted is more direct than the evidence based on the phenomenological model used to interpret the results of Donaghy and Stewart's long slit experiment. However, the two methods agree very well except for the enhanced value of the midposition count in this experiment. This discrepancy is not serious since it is probably due to the effect of the higher momentum components of the electron wavefunction and the width of the resolution function.

An examination of the higher momentum components of the electron wavefunction indicates that the observed anisotropy of 5.6% must be considered an upper limit to the true distortion of the Fermi surface of lithium. In this experiment the higher momentum components reduce the count rate in the <100> direction to a greater extent than in the <110> direction, and if this effect is corrected for, the experimental anisotropy is reduced

to 1.7%. In contrast, the higher momentum components of the positron are too small to have a significant effect on the anisotropy.

It is interesting to note that theoretical calculations are fairly consistent in predicting 5% bulges towards the zone boundaries in the <110> directions, whereas Compton x-ray experiments were unable to resolve any anisotropy within an accuracy of 3%. In addition, experiments on other alkali metals have shown that the Fermi surfaces of these metals are considerably less distorted than predicted by the extensive calculations of Ham. The positron annihilation studies constitute the only experimental evidence for a 5% distortion in the Fermi surface of lithium, yet it is apparent that this may partially be caused by the deviation of the electron wavefunction from a single plane wave. It is virtually certain that the distortion is not large enough to cause contact with the first Brillouin zone boundary in the <110> direction.

Concerning future work in this area, the most important requirement is an improved method of determining the effect of the higher momentum components on the coincidence count rates, preferably in a manner which does not require the prior selection of a crystal potential.

A logical extension of the lithium experiment would be to investigate lithium-magnesium alloys. It is known that up to 70 at.-% of magnesium can be added to lithium with no change

in the body-centred cubic structure and only small changes in the lattice constant. Positron annihilation experiments by Stewart[66] in polycrystalline Li-Mg samples show that it is a nearly free electron alloy. Experiments in single crystals would be of considerable interest since the free electron sphere of lithium expands with the addition of magnesium until contact occurs with the Brillouin zone face. A study of this effect would be valuable because the Li-Mg alloys are the simplest to treat theoretically.

APPENDIX I

Calculation of the Higher Momentum Components of the Electron Wavefunction Using the Method of Stroud and Ehrenreich[18]:

In M.K.S. units, the potential $V(\underline{r})$ seen by a positron moving in the Coulomb field of the electrons and nuclei is given by

$$V(\underline{r}) = \frac{1}{4\pi\varepsilon_o} \int \frac{\rho(\underline{r}')\, d\underline{r}'}{|\underline{r} - \underline{r}'|} , \qquad \text{A.1}$$

where the total charge density $\rho(\underline{r})$ is a sum of the nuclear and electronic charge densities:

$$\rho(\underline{r}) = \rho^{+}(\underline{r}) + \rho^{-}(\underline{r}) . \qquad \text{A.2}$$

Both $V(\underline{r})$ and $\rho(\underline{r})$ are periodic funtions with Fourier coefficients

$$V_{\underline{K}} = 1/v_a \int_{v_a} V(\underline{r})\, e^{i\underline{K}\cdot\underline{r}}\, d\underline{r} \qquad \text{A.3}$$

and

$$\rho_{\underline{K}} = 1/v_a \int_{v_a} (\underline{r})\, e^{i\underline{K}\cdot\underline{r}}\, d\underline{r} . \qquad \text{A.4}$$

The volume of a unit cell is denoted by v_a. Using the fact that these Fourier coefficients are nonzero only at reciprocal lattice vectors $\underline{K}$, equations A.1 and A.2 can be transformed to

$$V_{\underline{K}} = \frac{1}{\varepsilon_o} \frac{\rho_{\underline{K}}}{K^2} \qquad \text{A.5}$$

$$\rho_{\underline{K}} = \rho^{+}_{\underline{K}} + \rho^{-}_{\underline{K}} . \qquad \text{A.6}$$

Thus one can obtain the Fourier coefficients of the potential seen by the positron if the charge density $\rho_{\underline{K}}$ can be determined. Treating the nuclear part of A.6 in terms of point charges Ze at each lattice site, it is evident that

$$\rho_{\underline{K}}^{+} = \frac{Ze}{v_a} \qquad \text{A.7}$$

The electron charge density $\rho_{\underline{K}}^{-}$, can be expressed in terms of the atomic scattering factor as

$$|\rho_{\underline{K}}^{-}| = \frac{e}{v_a} f \ . \qquad \text{A.8}$$

The atomic scattering factor, f, is defined as the ratio of the amplitude of the wave scattered by the atom to that scattered by a single electron. Values of f for lithium were obtained from the Metals Reference Book.[64] Although these values are theoretical, it is found that agreement with experimental form factors is generally good.[65]

It is evident that the sign of $\rho_{\underline{K}}^{-}$ in equation A.8 must be negative since $-Ze/v_a$ is simply the average electron charge density. Incorporating the results of A.6, A.7, and A.8 into equation A.5 it follows that

$$V_{\underline{K}} = \frac{e}{\varepsilon_o v_a} \frac{(Z - f)}{K^2} \ . \qquad \text{A.9}$$

However, calculations are performed more easily if A.9 is expressed in atomic units so that $V_{\underline{K}}$ in rydbergs is given by

$$V_{\underline{K}} = \frac{1}{v_a} \frac{(Z - f)}{K^2} \qquad \text{A.10}$$

For a body-centred cubic crystal the volume of the unit cell is $v_a = 1/2(a^3)$ where the lattice constant 'a' is taken as 6.5183 a.u. The two shortest reciprocal lattice vectors which give rise to nonvanishing coefficients are

$$K_{110} = 2\sqrt{2}\pi/a \quad \text{and} \quad K_{200} = 4\pi/a \ .$$

The values of f are given for values of $\sin\theta/\lambda$ from 0.0 to 1.1 (λ in Å), therefore it is necessary to determine $\sin\theta/\lambda$ for (110) and (200) reflections in lithium. This is easily accomplished using the Bragg relation $2d\sin\theta = n\lambda$, and it is found that $\sin\theta/\lambda = 0.205$ for a (110) reflection and $\sin\theta/\lambda = 0.290$ for a (200) reflection. Th interpolated values of f are 1.79 and 1.54 respectively.

With this information the calculation of $V_{\underline{K}}$ is straightforward, and the following values are obtained for the first four coefficients:

$$V_{110} = 0.1182 \text{ Ry.}$$
$$V_{200} = 0.0713 \text{ Ry.}$$
$$V_{211} = 0.0295 \text{ Ry.}$$
$$V_{220} = 0.0178 \text{ Ry.}$$

BIBLIOGRAPHY

1. S. DeBenedetti, C.E. Cowan, W.R. Konnecker, and H. Primakoff, Phys. Rev. 77, 205 (1950)
2. J.J. Donaghy, Ph.D. thesis, University of North Carolina, (1964), unpublished
3. J.J. Donaghy and A.T. Stewart, in Low Temperature Physics, LT9, edited by J.G. Daunt, D.O. Edwards, F.J. Milford, and M. Yaqub, (Plenam Press Inc., New York, 1965), page 835
4. J.J. Donaghy and A.T. Stewart, Phys. Rev. 164, 391 (1967)
5. J.M. Ziman, Principles of the Theory of Solids, (Cambridge University Press, Cambridge, 1964)
6. The Fermi Surface, edited by W.A. Harrison and M.B. Webb, (John Wiley & Sons, Inc., New York, 1960)
7. M. Deutsch and S. Berko, in Alpha-, Beta-, and Gamma-ray Spectroscopy, Vol. II, edited by K. Siegbahm, (North-Holland Publishing Co., Amsterdam, 1965), page 1583
8. Positron Annihilation, edited by A.T. Stewart and L.O. Roellig, (Academic Press, Inc., New York, 1967)
9. Solid State Physics, Vol. I, Electrons in Metals, edited by J.F. Cochran and R.R. Haering, (Gordon & Breach Science Publishers Inc., New York, 1968)
10. G.E. Lee-Whiting, Phys. Rev. 97, 1557 (1955)
11. H. Weisberg and S. Berko, Phys. Rev. 154, 249 (1967)
12. J.P. Carbotte and H.L. Arora, Can. J. Phys. 45, 387 (1967)
13. S.M. Kim, A.T. Stewart, and J.P. Carbotte, Phys. Rev. Lett. 18, 385 (1967)

14. S. Kahana, Phys. Rev. 129, 1622 (1963)

15. J.P. Carbotte and S. Kahana, Phys. Rev. 139, A213 (1965)

16. J. Melngailis and S. DeBenedetti, Phys. Rev. 145, 400 (1966)

17. P.E. Mijnarends, Phys. Rev. 160, 512 (1967)

18. D. Stroud and H. Ehrenreich, Phys. Rev. 171, 399 (1968)

19. C.K. Majumdar, Phys. Rev. 140, A227 (1965)

20. P. Columbino, B. Fiscella, and L. Trossi, Nuovo Cimento 27, 589 (1963)

21. K. Fujiwara and O. Sueoka, J. Phys. Soc. Japan 21, 1947 (1966)

22. D. Ll. Williams, E.H. Becker, P. Petijevich, and G. Jones, Phys. Rev. Lett. 20, 448 (1968)

23. O. Sueoka, J. Phys. Soc. Japan 23, 1246 (1967)

24. W.A. Harrison, Pseudopotentials in the Theory of Metals, (W.A. Benjamin, Inc., New York, 1966)

25. C. Kittel, Quantum Theory of Solids, (John Wiley & Sons, Inc., New York, 1964), chapter 13

26. J. Callaway, Energy Band Theory, (Academic Press Inc., New York, 1964), chapter 2

27. C. Herring, Phys. Rev. 57, 1169 (1940)

28. H. Schlosser and P.M. Marcus, Phys. Rev. 131, 2529 (1963)

29. F. Seitz, Phys. Rev. 47, 400 (1935)

30. E. Wigner and F. Seitz, Phys. Rev. 43, 804 (1933)

31. M.L. Glasser and J. Callaway, Phys. Rev. 109, 1541 (1948)

32. J. Callaway, Phys. Rev. 124, 1824 (1961)

33. J. Callaway, Phys. Rev. 131, 2839 (1963), Erratum

34. F.S. Ham, Phys. Rev. 128, 82 (1962)

35. F.S. Ham, Phys. Rev. 128, 2524 (1962)

36. E. Antoncik, Czech. J. Phys. 10, 22 (1960)

37. V. Capek, Czech. J. Phys. B 18, 313 (1968)

38. V. Heine and I. Abarenkov, Phil. Mag. 9, 451 (1964)

39. M.H. Cohen and V. Heine, Adv. in Phys. 7, 395 (1958)

40. J.M. Ziman, Electrons and Phonons, (Oxford University Press, London, 1963), page 111

41. J.F. Cornwall and E.P. Wohlfarth, Nature 186, 379 (1960)

42. I.M. Templeton and K. Okumura, Bull. Am. Phys. Soc. 9, 239 (1964)

43. J. Melngailis and S. DeBenedetti, Phys. Rev. 145, 400 (1966)

44. H. Stachowiak, to be published, 1970

45. M. Cooper, J.A. Leake, and R.J. Weiss, Phil. Mag. 12, 797 (1965)

46. W.C. Phillips and R.J. Weiss, Phys. Rev. 171, 790 (1968)

47. M. Cooper, B.G. Williams, R.E. Borland, and J.R.A. Cooper, Phil. Mag. 22, 441 (1970)

48. D. Shoenberg and P.J. Stiles, Proc. Roy. Soc. (London), A281, 62 (1964)

49. D.E. Bedo and D.H. Tomboulian, Phys. Rev. 109, 35 (1958)

50. R.G. Chambers, in reference 9, page 332

51. T. Suzuki, J. Phys. Soc. Japan, 22, 1139 (1967)

52. A.W. Hull, Phys. Rev. 10, 689 (1917)

53. H.C. Nash and C.S. Smith, J. Phys. Chem. Solids 9, 113 (1959)

54. G. Champier, Bull. Soc. Franc. Miner. Crist. LXXXII, 61, (1959)

55. J. Trivisonno and C.S. Smith, Acta Metallurgica 9, 1064 (1961)

56. T. Slotwinski and J. Trivisonno, J. Phys. Chem. Solids 30, 1276 (1968)

57. R. Feder, Phys. Rev. 2B, 828 (1970)

58. E. Mantysalo, Ann. Acad. Scient. Fennicae AVI 178, 22 (1965)

59. M. Majima and S. Togino, Scientific Papers of the Institute of Physical and Chemical Research (Japan) 7, 259 (1927)

60. J. Shiller, J.W. Dooley, N. Tepley, R.L. Thomas, and J. Fenner, The Review of Scientific Instruments 41, 51 (1970)

61. P. Petijevich, M.Sc. thesis, University of British Columbia, (1967), unpublished

62. E.H. Becker, Ph.D. thesis, University of British Columbia, (1970), unpublished

63. J.H. Terrell, H.L. Weisberg, and S. Berko, in reference 8, page 269

64. Metals Reference Book, Vol.I, edited by C.J. Smithells, (Butterworth and Co., London, 1967), page 121

65. B.W. Batterman, D.R. Chipman, and J.J. DeMarco, Phys. Rev. 122, 68 (1961)

66. A.T. Stewart, Phys. Rev. 133, A1651 (1964)